DESIGN AND DEVELOPMENT OF 89C51 BASED ELECTRICAL IMPEDANCE TOMOGRAPHY SYSTEM

A Dissertation Submitted in Partial Fulfilment of the Requirements

For the Award of Degree of

Master of Engineering

In

Electronics Instrumentation and Control

Submitted by

Udayan J Trivedi

Regd. No 801151029

Under the Guidance of:

Dr T.K. Saxena
Chief Scientist and Head
Vibration, Ultrasonic and Acoustic Standard and Electronics and Instrumentation Cell
CSIR-National Physical Laboratory
Dr. K. S. Krishnan Road
New Delhi- 110 012

Dr. Ravinder Agarwal
Professor,
Department of Electrical and Instrumentation Engineering
Thapar University, Patiala
Punjab

Department of Electrical and Instrumentation Engineering
Thapar University
(Established under the section 3 of UGC act, 1956)
Patiala, 147004, Punjab, India

July 2013

DECLARATION

I hereby certify that the work which is being presented in the thesis entitled, **"DESIGN AND DEVELOPMENT OF 89C51 BASED ELECTRICAL IMPEDANCE TOMOGRAPHY SYSTEM"** in partial fulfilment of the requirements for the award of degree of masters of engineering in Electronics Instrumentation and Control Engineering Department, Thapar university, Patiala, is an authentic record of my own work carried out under the supervision of **Dr T.K. Saxena**, Chief Scientist National Physical Laboratory, New Delhi and **Dr. Ravinder Agarwal**, Professor, Department of Electrical and Instrumentation Engineering, Thapar University, Patiala,Punjab.

Date: 04/07/2013

Udayan J Trivedi

Roll No 801151029

I certify the above statement made by the candidate is correct and true to best of my knowledge and belief.

Date:

T.K. Saxena

Dr. T.K. Saxena
Chief Scientist and Head
Vibration, Ultrasonic and Acoustic
Standard and Electronics and
Instrumentation Cell
CSIR-National Physical Laboratory
Dr. K. S. Krishnan Road
New Delhi- 110 012

Agarwal

Dr. Ravinder Agarwal
Professor,
Department of Electrical and Instrumentation Engineering Thapar University, Patiala
Punjab

Countersigned by:

S. Ghosh

Dr. Smarajit Ghosh
Head of Department
Department of Electrical and
Instrumentation Engineering
Thapar University, Patiala
Punjab

Dr. S.K. Mohapatra
Dean of Academic Affairs
Thapar University, Patiala
Punjab

Acknowledgement

With deep sense of gratitude I express my sincere thanks to my esteemed and worthy supervisors, **Dr T.K. Saxena**, Chief Scientist and Head Vibration, Ultrasonic and Acoustic Standard and Electronics and Instrumentation Cell. NPL New Delhi and **Dr Ravinder Agarwal**, Professor, Department of Electrical and Instrumentation Engineering, Thapar University, Patiala for their valuable guidance in carrying out this work under their effective supervision, encouragement, enlightenment and cooperation Most of novel ideas and solutions found in this thesis are the result of our numerous stimulating discussions. Their feedback and editorial comments were also invaluable for writing of this thesis.

I express my sincere thanks to Prof. R. C. Budhani Director NPL for providing me the opportunity to work at the NPL. I would also like to thanks Dr. Rajeev Chopra, Head HRD, NPL and Mr. Dharamvir, HRD NPL for their support and guidance.

I shall be failing my duties if I do not express my deep sense of gratitude towards **Dr.Smarajit Ghosh**, Professor and Head of the Department of Electrical and Instrumentation Engineering, Thapar University, Patiala who has been a constant source of inspiration for me throughout this work.

I am also thankful to Mr Aveneesh Mittal, Ms. Priyanka Jain and Ms. Poonam Sethi Bist for their full co-operation and timely help.

A special thank is to my beloved family, to my mother, my brother and sister for their unlimited love and support.

Finally, I would dedicate this work to my father, my spiritual support, the most solicitous person to my M.E. Dissertation but can never see this moment. Because of him, I did not give up even in the hardest time.

Place: Thapar University, Patiala

Udayan J Trivedi
801151029

Abstract

Electrical Impedance Tomography is an imaging technique used in Medical, Industrial and Geophysical fields for imaging the interior parts of human body, process control, looking beneath the earth respectively. The subject of this dissertation is the design of the Data Acquisition electronics for use in a medical imaging system based on Electrical Impedance Tomography (EIT). And make the software to reconstruct the conductivity distribution image. The data is required to be sufficiently accurate to allow the successful image of absolute conductivity.

In this dissertation work the EIT system is Designed and developed around Microcontroller 89C51 and op-amp based constant current source. The data acquisition system and the image reconstruction program were developed on VB.10 and EIDORS tool kit for MATLAB R2011a. The system was tested on the 2D phantom to see the ability of the system to reconstruct the 2D image of the phantom. The different imaging algorithms are implemented and compared to reconstruct the image. The developed system can be used as a prototype in the laboratory for the evaluation of EIT technique.

Table of Content

List of Figures

List of Tables

CHAPTER ONE

Electrical Impedance Tomography: An Introduction

1.1 Introduction to Electrical Impedance Tomography

Electrical Impedance Tomography (EIT) belongs to a family of electromagnetic imaging modalities along with techniques such as Electrical Capacitance tomography (ECT) [1] electromagnetic tomography (EMT) [2] and magnetic induction tomography (MIT) [3]. It is a technique used to create images of the electrical properties in the interior of a body from measurements on its boundary. Usually, a set of voltage measurements is acquired from the boundaries of a conductive volume, whilst this is subjected to a sequence of low-frequency current patterns. In principle, measuring both the amplitude and the phase angle of the voltage can result in images of the electrical conductivity and permittivity distributions in the interior of the volume. Despite the fact that electrostatic fields are ideally required, alternating current patterns are often preferred in order to avoid polarization effects. In this frequency range (less than 100 KHz), the magnetization components of the current are negligible and the phase angles are maintained relatively small, thus usually the real part of the voltage is a few hundred times greater than the imaginary. In the absence of phase angle reading in the data, only the conductivity (or equivalently the resistivity) distribution can be reconstructed, and the technique is transformed to its simplified equivalent electrical resistance tomography (ERT). For simplicity, the term 'admittivity' is used to describe the complex electrical property of a conductive volume, whose real and imaginary parts are measures of the conductivity (σ) and scaled permittivity ($\omega\epsilon$) at a given point inside the volume. A typical EIT system is compact set of equipment mainly consisting of the data acquisition unit with the current source and the sensors attached, and a computer with the reconstruction code on board.

'Soft-Field' modalities such as EIT are intrinsically difficult compared to 'Hard-Field' techniques like X-rays computer tomography (CT) for instance, widely established in high resolution imaging [4]. In an X-ray CT scanning process, parallel beams of X-rays are guided into the body under test form a suitable source while some detectors measures the attenuated beam as these emerges from the body. This procedure is repeated, rotating both sources and detectors around the body under test. In sequence, images of the attenuation coefficient distribution inside the body are developed using algebraic or analytic reconstruction algorithms. These appear to be extremely efficient for this particular reconstruction problem

in terms of its computational speed and the spatial solution of the image. This is mainly because X-rays propagate in straight lines through the body. Their absorption at any point inside the boy is completely independent of the absorption at any other point. The geometrical arrangement for X-ray CT is to measure the attenuation along each collimated beam direction. This is in fact a linear problem which leads to sparse and well-conditioned sensitivity matrices (radon transforms) and very large data sets. On the other hand, EIT and indeed any low-frequency electromagnetic radiation has such long wavelength that an electrostatic representation is most appropriate, describing the field throughout the body using a laplacian equation. It is inherent in this soft-field approach that the field strength at any point is a function of the distribution of the electrical properties throughout the body. As the field is modified throughout the body, the measured potential values at a given boundary location under a given excitation geometry is a non-linear function of the distribution of the electrical parameters throughout the body. This makes the associated reconstruction problem less easy to solve if not problematic.

The relatively poor spatial resolution of the reconstruction image in impedance tomography is often quoted as its major disadvantage, compared with already established scanners with good resolution. In this respect, it must be clarified that the motivation for EIT is somewhat different from that of the conventional imaging modality. Despite its limited resolution, its task is to provide a reliable, real-time, portable and cost efficient imaging tool, targets unfortunately met at the expense of high quality images. The spatial resolution is severely affected by the ill-posedness of the imaging reconstruction problem, in the sense that even large improvements in the measurements can only manage minor enhancements in the quality of the images. In an abstract way, the reconstructed image can be seen as a source of information aiming to answer certain questions about the interior electrical properties of a particular volume. In this context, an image of a reasonable low resolution is therefore a limited source of information. However, its value and utility are still dependent on the actual question to be asked by the user. Depending on the particular application and the resolution specifications, EIT can sometimes provide the optimum cost effective imaging solution. At present, its main application areas include

1. *Industrial*: These applications include the imaging of fluid flows in pipelines, the measurement of fluid distribution in mixing vessels, and non-destructive testing such as crack detection [5, 6].

2. *Geophysical:* Applications include geophysical prospecting, cross borehole measurement and surface measurement [7, 8].

3. *Medical*: EIT is used for monitoring of pulmonary and cardiac functions, measurement of brain function, detection of haemorrhage, measurement of gastric imaging, detection and classification of tumours in breast tissue and functional imaging of the thorax [9, 10, 11, 12, 13, 14, 15, 16].

Image reconstruction in EIT appears to be the more challenging compared to that of the hard-field imaging modalities, and in some respects this may also be seen as a disadvantage. The vast majority of existing numerical EIT algorithms necessitate the calculation of sensitivity matrix which relates interior admittivity perturbation to perturbation in the boundary data, but among them there is a large diversity as to the way this matrix is handled. By default, the sensitivity matrix, which is simply the jacobian of the discrete forward operator, is heavily ill-conditioned with respect to inversion and as such it requires special treatment usually in the form of regularization or a truncation of a singular value expansion.

As far the on-site installation and performance of EIT is concerned, not many will argue about its reliability in operating with high speed under harsh industrial environments. Already installed systems in industrial plants at Syngenta and DuPont have recently reported some encouraging results. Costing only a fraction of the price for a moderate CT scanner, EIT's compact equipment makes it a portable imaging tool which can easily fit within an industrial production line for process control, or an operating theatre for real-time patient monitoring.

CHAPTER TWO
Literature Review

2.1 Introduction

Electrical Impedance Tomography (EIT) is a technique for mapping the distribution of electrical conductivity (real or complex) within some medium. The conductivity information is obtained from measurement of voltage and/or current on the periphery of the region as a result of externally applied voltages or currents. Images are obtained from the peripheral data with the use of an algorithm. Human body tissues display a wide range of conductivities [17] and hence the potential exists to use EIT to carry out medical imaging using conductivity as the parameter to be mapped. Much research has been carried out during the last fifteen years on applying EIT as a medical imaging system.

The design of a generalised medical EIT system is illustrated in Figure 2.1 and comprises a set of electrodes applied to the patient, usually arranged equidistantly around the circumference of the region within a single plane, a data acquisition system and a computer executing an algorithm to reconstruct impedance images from data obtained by the data acquisition system. Some systems are capable of adapting the applied stimulus to suit the impedance distribution within the image plane. Typically, the system generates a 2D cross-sectional image at the electrode plane.

Alternating current (AC), rather than direct current (DC), is used for several reasons. DC applied to the skin causes electrolytic action under the electrode and may result in ulcers [18]. The maximum AC current that may safely be applied is frequency-dependent with the maximum current increasing linearly with frequency between 1 kHz and 100 kHz [19]. The voltage data accuracy improves with larger applied currents because larger currents result in larger measured voltages and hence a greater signal-to-noise ratio. This implies that the use of higher frequencies may result in more accurate data. In contrast, the accuracy of the data acquisition system may become degraded at higher frequencies due to the effects of parasitic capacitances. The most popular frequency range is about 10kHz to 1000kHz [20,21,22,23,24,25,26,27,28,29,30] although the system by Cusick et al. [31] operates down to 100Hz.

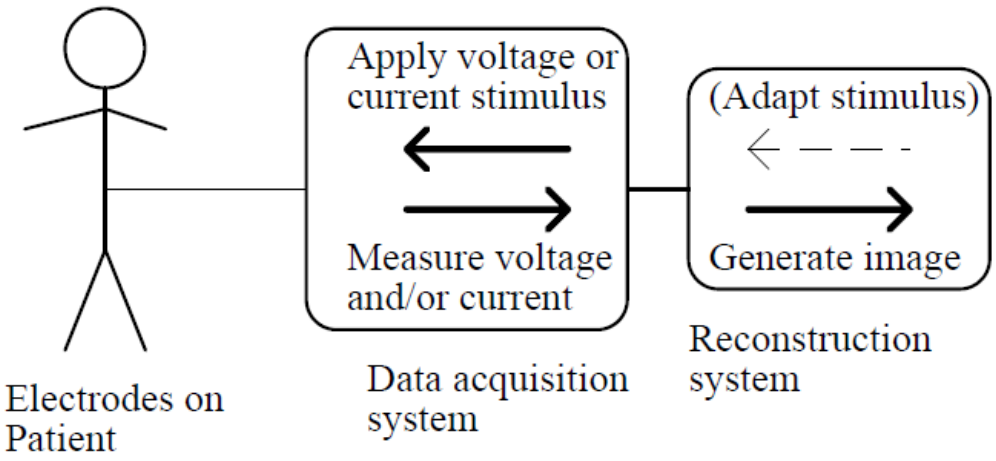

Figure 2.1: Generalised EIT System.

Research into EIT is driven by the fact that some medical conditions exist for which EIT may have advantages over other existing imaging techniques. Clinical examination and X-rays, for example, are insensitive to vascular distension associated with pulmonary oedema and EIT has been suggested as a possible imaging method [32]. EIT might permit continuous monitoring for intraventricular haemorrhage in premature infants [33]. Tissue conductivity is affected by temperature [34] and therefore the monitoring of tissue conductivity by EIT may potentially be used to monitor tissue temperature during hyperthermia therapy. This method would replace the invasive planting of a thermocouple. The conductivity of blood is known to change with flow rate [35], possibly allowing flow-rate measurements such as cardiac output to be determined. In addition, the presence of air, blood or other fluid in an organ may affect the overall conductivity and hence may be detectable. An EIT system has been proposed for the localisation of epilepsy using the variation in brain tissue conductivity due to abnormal brain activity [36]. EIT has been suggested as a means of monitoring gastric function as an alternative to dye dilution or gamma camera methods [37].

EIT has more general advantages over other imaging techniques, such as relatively low cost (as developed hardware, described in this dissertation, was approximately Rs1000-1500) in comparison with other tomographic methods, compactness, due to the absence of large transducers and ease of integration of a purely electronic system, and safety in comparison with X-ray methods.

The speed of image production is limited by the speed of the data acquisition system and the reconstruction algorithm. Data acquisition and reconstruction which is fast enough to allow video-rate imaging has long been achieved using the back-projection method [38]. Non-backprojection methods have recently become fast enough to acquire data and reconstruct at near video rates. EIT offers the potential to meet the requirements for a safe, low-cost real-time imaging system which provides good contrast between tissues.

EIT does, however, have its own limitations. These include low resolution, due to the limited number of independent measurements that are practical, and inability to probe enclosed high impedance layers, such as the adult skull, unless some surgery is performed to allow instrumentation to gain access to the brain. An exception to the latter case is that of the neonatal skull which has a sufficiently low impedance to allow cerebral imaging [17]. EIT is therefore most applicable to measurement of the conductivity of relatively large tissue regions, or of blood, air or other fluid content of such tissues, and the measurement of changes in these parameters with time.

2.2 History of EIT

In the first impedance imaging system of 1983, the impedance camera, was constructed by Henderson and Webster [40] to study pulmonary oedema which had proven difficult to measure using single-channel impedance instruments. It was hoped that the use of multiple channels would allow more localised impedance measurements. The system used a rectangular array of 144 electrodes placed on the chest with a single large electrode placed on the back. Electrodes were driven with a 100 kHz voltage signal and currents were measured on each electrode sequentially. A conductivity contour map was produced based on the assumption that currents flowed in straight lines through the subject, and which showed a conductivity variation caused by the lungs. The image showed relatively low conductivity regions corresponding to the locations of the lungs with a minimum to maximum contrast of approximately 2.5:1.

In the early eighties, Barber and Brown [17] began work on electrical impedance imaging. Their relatively simple system used 16 electrodes and applied a constant current at 50 kHz to only two electrodes at a time [41]. Differential voltages were recorded from adjacent electrodes. Data was recorded at a rate sufficient to generate 10 images per second. The images were computed using a method known as back-projection. This method had been used

with great success in the field of X-ray tomography and it was realised that for small conductivity variations from the uniform case, the electrical impedance images could be reconstructed in a similar method to those of X-ray tomographic imaging. The reconstruction algorithm used normalised voltage change between two sets of data recorded at different times, rather than absolute voltages, because measurement errors due to, for example, electrode position are claimed to be reduced with this approach. The first set of data is termed the “reference set”. The system was thus limited to difference imaging. The process was named Applied Potential Tomography and results were published in 1982 showing an image derived from the human arm [42]. The image was obtained by immersing the arm into a saline-filled tank which supported the electrodes. The reference data set was the data from the tank without the arm present. The image appeared to show the bones, the muscular tissue, and two blood vessels. The resolution of the image was, however very low. This image is generally regarded as the first successful in vivo image generated by an EIT system.

Images of the lungs and of gastric function [43] were later published. The images showed the passage of tap water into the stomach and of conductivity changes in the lung regions during respiration. As the images are dynamic, only the part of the stomach filling with water is visible in the gastric image, and the inflating lungs are the only visible features of the lung images. The lung images obtained from a patient with known lung water showed reduced conductivity change in the affected lung, as would be expected. The images are scaled in units of log resistivity change and the resolution is low. Studies were undertaken to assess the accuracy of the gastric function images and good correlation with other methods was obtained [37]. Experiments were also undertaken to assess the system's use for monitoring respiration [44], cardiac functions [45], hyperthermia [46], and intraventricular haemorrhage in low-birth weight neonates [33]. Although the experiments produced images of the required function, the resolution remained low at 10% of the diameter of the observed region.

At the same time, work progressed on alternative reconstruction algorithms, such as the perturbation method [47] and the Newton-Raphson method. Yorkey and Webster [48] concluded that the Newton-Raphson method was the best of the existing iterative EIT reconstruction techniques in one-step correction and in image accuracy for a given number of iterations. Tarrasenko and Rolfe [49] suggested the application of EIT techniques to studies of the monitoring of intraventricular haemorrhage (IVH) in neonates. Work was undertaken on a Sheffield-type system with the particular application of monitoring IVH and other

potential problems in neonates. Results were published in 1987 [33] showing conductivity change in the stomach of an adult using the Sheffield reconstruction algorithm.

2.3 Back-projection Based System.

Since the mid 1980's, interest in EIT has grown considerably. A number of European research groups have adopted the back-projection algorithm. A recent trend is the use of back-projection at multiple frequencies and the use of data from one frequency as the reference against which data at other frequencies may be imaged [50, 25, 23].

In 1989, this method was used to produce a frequency-based differential image of the abdomen and in, 1990, of the forearm [28]. The forearm image demonstrated that the significant change in muscle conductivity with frequency between 40 kHz and 80 kHz causes muscle tissue to be clearly imaged. The possibility of imaging change in conductivity phase angle was demonstrated in 1991 using both a resistive phantom and an *in vivo* measurement of the thorax [51]. The lungs were clearly imaged with the real component data but a different pattern was observed with the imaginary component which may have been due to the effect of other organs near the image plane.

In 1988 Rosell designed a multi-frequency system which simultaneously applied two frequencies. In vivo frequency difference images of a human thigh for the real and imaginary components were published in 1992 [52]. These images again showed that muscle tissue exhibits the largest conductivity variation and were clearly imaged. The imaginary part of the data showed greatest contrast between muscle and bone.

Gersing and Osypka [30] showed that, when imaging the lower leg with the dual frequency method, better resolution of muscle may be obtained if the imaginary parts of the conductivity or the time constant are imaged. The method used 10 kHz and 20 kHz excitation with 16 electrodes. In 1987 in vitro and in vivo studies were carried out into the feasibility of imaging local temperature changes using EIT in order to monitor hyperthermia therapy [34]. EIT may be used for this because tissue conductivity is known to change with temperature. The human thigh was imaged and heated by approximately 7.5°C using a radio-frequency method. Changes in conductivity were clearly visible although the heating occurred near the surface where imaging is least problematic.

The back-projection method has also been applied to imaging the act of swallowing with the aim of assessing dysphagia (impaired swallowing) [53]. Images were produced of a cross-section of the neck, and the passage of tap water during swallowing has been imaged.

As mentioned in [54] Holder and others have researched, since 1987, the use of back-projection based EIT in many applications including imaging the brain with the intention of detecting regions of abnormal neuronal activity. One application is for localising epileptic foci so that the correct region may be surgically removed [36]. Experiments on animals have demonstrated the feasibility of the method and have also shown that localised brain activity as the result of sensory stimuli may be imaged [55].

In 1990 Smith introduced the Sheffield mk2 system [38] which included digital demodulation and had a faster data acquisition speed (25 data sets per second). The system retained the same 16-electrode configuration and used a 20 kHz operating frequency. In vivo images were obtained on-line and lung ventilation and cardiac cycle images could be generated separately, using a temporal filtering technique [56]. The images produced were, however, still of conductivity change rather than absolute conductivity. As well as imaging in real-time, the system could also be used to separate features, such as the lungs and the heart, on the basis of temporal frequency.

In 1992 Barber and Brown began work on a multi-frequency tomograph, called Mark-3, which operated at seven frequencies between 9.6 kHz and 614 kHz. Results were published in 1994 showing EIT images of the lungs based on the parameters of conductivity variation with frequency [38]. The images are similar to those obtained of conductivity change in form and resolution.

2.4 Non Back-projection System

In contrast to the European trend, Gisser, Newell and Isaacson of the Rensselaer Polytechnic Institute (RPI) were the first to adopt an adaptive, multiple-drive approach to EIT. In 1987 the term 'distinguishability' was introduced [57] to describe the ability of certain current pattern to generate changes in the boundary voltages for a certain conductivity distribution. The best, or optimum pattern produces the largest change in boundary voltages for a given conductivity distribution in comparison with a uniform distribution. The generation of optimum current patterns requires an EIT instrument capable of applying currents of

independently controllable amplitudes to all current electrodes simultaneously. The instrument must therefore be more complex than one designed for back-projection which applies a pair of currents of fixed amplitude.

Work also began at Oxford Brookes University [58] on the mathematics of EIT reconstruction. This work was prompted by research into the feasibility of using EIT to detect cerebral haemorrhage in the new-born. Interest developed in the use of optimal currents which led to the design and construction of an optimal current tomograph OXPACT 1.

In 1988 Newell and Isaacson published results of distinguishability tests on a multiple-drive tomograph (ACT 1) [59] which used 32 electrodes and operated at 12kHz. Phantom images were published the same year which were obtained from a second tomograph ACT 2 [36], again using 32 electrodes and the same configuration but operating at 15 kHz. The system required 30 seconds to obtain one data set. The phantom image of a conductive cylinder in a saline solution had a similar low resolution to those produced by the Sheffield system and were obtained by subtracting images obtained from the phantom with and without the targets present.

In 1990 Cheney and Isaacson published details of the one-step reconstruction algorithm NOSER along with images from a phantom and images of both absolute conductivity and of conductivity change from a human thorax [60]. The thorax images were of low-resolution and showed the lungs and possibly the ribs, although little detail can be seen.

The third generation tomograph ACT 3 was introduced by Newell and Isaacson in 1991 [61]. Once again 32 electrodes are used and the voltages are measured on the current-carrying electrodes, however the system is much faster, generating 7 data sets per second and digital demodulation is employed. The system has a high degree of parallelism to obtain a high data acquisition speed through the utilisation of a dedicated digital signal processor for each channel. The system can also carry out self-calibration in which the finite parasitic impedances at the electrodes are cancelled out by the application of negative real and imaginary impedances. The system also permits multi-frequency measurement by operating a 7.5 kHz, 15 kHz and 30 kHz. Absolute conductivity images of the chest using the ACT 3 system were published in 1992 [62]. These images show regions where conductivity changes with respiration, which may be attributed to the lungs. The images are very different in

appearance from those obtained from the Sheffield systems and do not show the lung outlines as clearly. The central region of the image has a relatively high conductivity.

2.5 EIT Reconstruction

EIT is distinct from other tomographic techniques in that the reconstruction is complicated by the fact that electric current is not confined to a narrow beam, as with collimated gamma or X-radiation, but spreads out over the entire region to be imaged. The reconstruction method therefore is more difficult to implement and more prone to error. This chapter describes the reconstruction problem and some reconstruction methods used or suggested for use with EIT in the section 2.7.

2.6 Mathematical Basis

The feature which distinguishes EIT from other methods is that the applied signal generates a current vector field within the observed region for which the divergence is zero. This may be written as

$$\nabla \cdot J = 0 \tag{2.1}$$

where J is a vector describing the current density at any point within the observed region. This may be regarded as a continuous version of Kirchhoff's current law. At any point within the region, the current density vector is the electric field vector E multiplied by the conductivity scalar s at that point, hence

$$\nabla \cdot (sE) = 0 \tag{2.2}$$

which is the continuous equivalent to Ohm's law. E is equal to the gradient of the potential at that point and hence

$$\nabla \cdot (s \nabla V) = 0 \tag{2.3}$$

With a uniform resistivity distribution s is constant and hence the corresponding expression with voltage V_U is

$$\nabla^2 V U = 0 \tag{2.4}$$

2.7 Reconstruction Method

To reconstruct an image of conductivity distribution it is necessary to solve (2.3) to obtain s. This problem can be solved analytically for simple conductivity distributions but for arbitrary distributions as would be expected in medical imaging applications, this is not possible. In many EIT systems, the approach to solving (2.3) for conductivity involves breaking down the region of interest into a finite number of regions in which the conductivity may be specified simply. A relationship may be obtained between the voltage measurements made on the boundary and the conductivities of such regions. If there are N such regions then N simultaneous equations can be made to define the dependence of the conductivity values on the boundary measurements. This may be expressed as:

$$v = F.c \tag{2.5}$$

where c is a vector of conductivity values, v is the vector of voltage measurements and F is the transformation relating v to c. If F and c are known, this is easy to solve and is known as the “forward problem”.

EIT seeks to find a relationship:

$$c = F^{-1}.v \tag{2.6}$$

Hence, values of v measured on the boundary are formed into a vector and applied to (2.6) to obtain c. This is known as the “inverse problem”. However, simple inversion of F is not possible because F is a non-linear transformation and cannot therefore be inverted by standard matrix methods. One solution is to assume that, for small variations from the uniform case, F may be approximated as linear and may then be inverted. The inversion of F is however error-prone. N cannot be greater than the number of linearly independent voltage measurements used to probe the region, which is the product of the number of voltage measurements per applied current pattern and the number of patterns divided by two.

2.7.1 Back-projection Method

Back-projection in EIT [17] follows similar principles to that of X-ray tomography. A finite number of electrodes are applied to the periphery of the region to be observed. A current is applied to one electrode and is withdrawn from another. The resulting flow of current results in a distribution of potential throughout the observed region. The voltage distribution in a region of uniform conductivity when current is applied and withdrawn from adjacent electrodes will be similar to that shown in Figure 2.1. The equipotentials spread out from the driver electrode pair in a manner similar to dipole radiation.

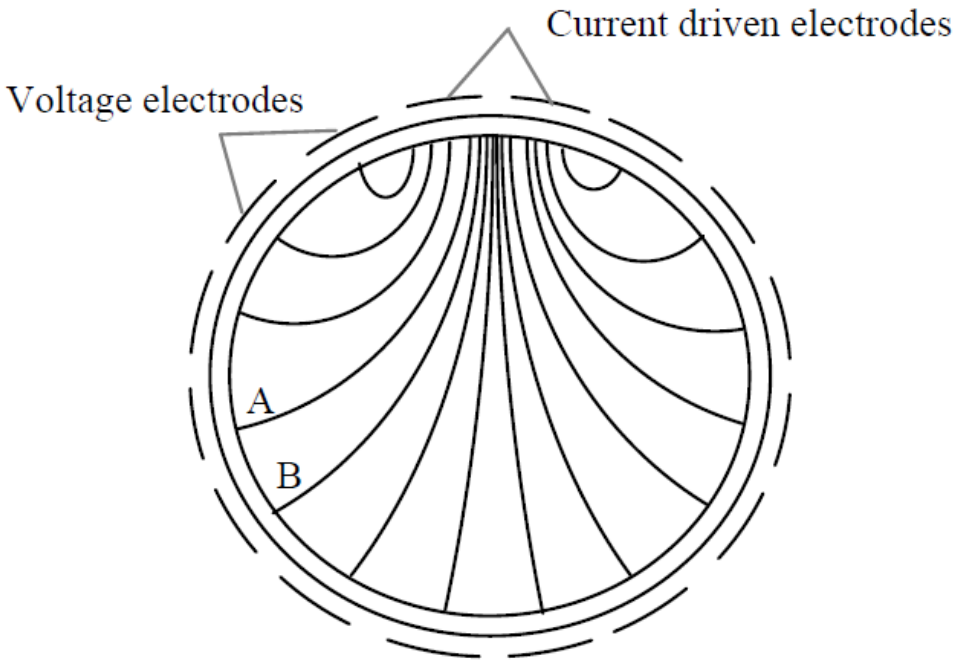

Figure 2.1: Equipotentials for a Pair-riven Homogenous Region.

The reconstruction method generates an image by the repeated summations of images of the regions between the relevant equipotentials which are weighted according to the voltage measurement concerned.

The measured differential voltages are clearly proportional to the electrode spacing and it has been stated [41] that the voltage measurement accuracy has to be of the order of 0.1%, which implies that the electrode spacings must be similarly accurate. This precision is not easy to achieve, especially if the common practice of placing the electrodes individually on the skin

is adopted. A further problem is the shape of the boundary, which for the human torso will certainly not be circular. These restrictions have made absolute imaging difficult. Successful results have, however, been obtained [32] by using a measured data set as a reference and back projecting normalised changes from this reference set instead of the absolute voltages. This approach greatly reduces the effects of the errors referred to above. This method is termed “difference imaging”.

The image quality may be improved by filtering the boundary voltage data set prior to reconstruction. A more recent development is the application of the back-projection algorithm to imaging change of conductivity with respect to excitation frequency instead of time. This permits a form of difference imaging where frequency dependence of conductivity is imaged [40, 25, 23].

The back-projection method is widely used by the European groups. It requires a relatively simple system design and reconstruction is computationally undemanding, but current is applied to adjacent electrodes because it was thought that this produced the best resolution [62]. This is a poor configuration in terms of signal to noise ratio [63] because relatively small differential voltages are produced in comparison with, for example, polar drive in which the driven electrodes are on opposite sides of the region. Only differential imaging, in terms of time or frequency, is carried out with this method.

2.7.2 Perturbation Method

The perturbation method [47] was an early attempt to apply Newton's method to EIT. A sensitivity matrix was constructed by changing the resistivity of one element at a time and forward modelling. This was then used as the derivative matrix of the boundary voltages with respect to the element resistivities. The measured boundary data was applied to the sensitivity matrix to determine a new set of resistivity values. The process was then repeated iteratively.

The perturbation method produces accurate images in simulations but convergence is slow in comparison with other methods. It is because the sensitivity matrix is computationally intensive to calculate and must be calculated again for each iteration. This technique is important historically as one of the first iterative methods to be used in EIT but is no longer in use.

2.3.7 Newton's Method

This method [64] seeks to minimise the mean of the squares of the voltage errors between those generated by a model and those measured from the observed region. The difference between the two values is sometimes termed the "objective function". The minimisation is achieved by obtaining the derivatives of the objective function with respect to resistivity. This derivative is assigned to zero, which corresponds to a local minimum of objective function. This would correspond to the conductivity which produces the boundary voltages closest to the measured voltages in the least-squares sense. A system of equations is therefore generated which when solved will give the closest approximation of resistivity in terms of the objective function.

Yorkey et al. [65] demonstrated that this reconstruction method converged faster than any of the other contemporary methods (the layer stripping algorithm was published later) and that the first iteration produced less error than the back-projection method.

If one step only is used, the initial derivatives based on the uniform distribution may be obtained analytically and need not be recalculated. The algorithm based on one step of the above method is termed NOSER [66].

The use of Newton's method for more than one iteration requires the solution of the forward problem for each iteration. This requires a considerable amount of computing time. An iterative algorithm POMPUS [67] was developed by Paulson which uses optimal current patterns (described below) and considerably reduces the computational complexity required for multiple iterations of Newton's method. This method greatly reduces the time needed to produce images and hence considerably eases the problem of performing iterative reconstruction in real-time.

2.7.4 Layer Stripping Method

This method was first described by Cheney et al [68]. The technique is unusual in that it reconstructs images from the periphery inward. Voltages and currents on the exterior surface are used to estimate the outermost layer of conductivity. Once this is determined, the outer layer is used in conjunction with the measured voltage and current values to determine the next layer inwards. The process is repeated until the algorithm reaches the centre of the

image. It is claimed that the method achieves a more accurate conductivity contrast than other methods.

2.8 Optimal Current

In order to maximise the resolution of the final image it is necessary to make as many independent measurements as possible. To achieve this a set of independent current patterns is applied to the boundary. The number of such patterns cannot exceed the number of current electrodes minus one but the patterns themselves may take any form provided that no one pattern can be formed by the linear combination of any of the others. Two popular choices are the trigonometric scheme and the pair-driven scheme. The trigonometric scheme applies a pattern of currents, the magnitudes of which are determined by

$$I\theta = A\ cos(n\theta)$$

$$1 \leq n \leq \frac{e}{2}$$

Or

$$I\theta = A\ sin(n\theta)$$

$$1 \leq n \leq \frac{(e-1)}{2} \qquad (2.7)$$

Where A is the maximum current, e is the number of current electrodes and θ is the angular position of the centre of the current electrode.

The pair-driven scheme applies current between adjacent electrodes. Only, the remaining electrodes supply no current and may be used for voltage measurement. This method requires simpler electronics than the trigonometric approach because only two current electrodes are driven at one time.

In 1987, Gisser et al [57] introduced the concept of “distinguishability” which is a quantitative measure of a current pattern's ability to maximise the mean square voltage

difference between two resistivity distributions. This concept is represented mathematically as:

$$d = \left[\frac{\int_S \left| \left(R(\sigma) - R(\tau) \right) j \right|^2 \, dA}{\int_S |j|^2 \, dA} \right]^{\frac{1}{2}} \tag{2.8}$$

Where d is the distinguishability, σ and τ are two resistivity distributions to be distinguished, S is the region to be observed, dA is an element of S and R is the linear operator mapping j onto the voltage measured on the periphery. σ and τ are said to be distinguishable if d > e where e is the measurement precision. Distinguishability is important because all real tomographs have noise present in the measured voltages, generated by quantisation and other sources, and hence data accuracy is optimised by maximising the measured voltage changes for a given homogeneity.

It was shown that the distinguishability for any resistivity distribution could be maximised by using a current pattern set which was tailored to that specific distribution, i.e. an optimal pattern set. Gisser et al also presented a simple iterative algorithm for obtaining an optimal current pattern and demonstrated it with a concentric distribution.

Breckon and Pidcock [69] showed numerically that the adoption of adaptive currents improved the accuracy of image reconstruction for one iteration of Newton's method. It was also claimed that adaptive currents reduced the errors due to boundary shape error.

2.9 Resolution

An important limitation of the system compared with X-ray tomography and of tomography systems in general, is the limited resolution of the final image. The resolution is dependent on the number of independent measurements which may be obtained from the region, which is in turn dependent on the number of electrodes. The resolution is also dependent on distance from the boundary. In 17 general, the resolution decreases away from the edge of the imaged region and is least in the centre of the image.

EIT requires static electrodes in contact with the skin and hence more projection angles can be achieved only by using a larger number of electrodes. The number of electrodes is restricted by trade-offs between the advantages gained by using physically large electrodes

in terms of reduced electrode impedance, and the limited space available on the circumference [70].

2.10 Hardware Requirements

The choice of reconstruction algorithm may have implications for the hardware design of the system. The back-projection method applies currents to adjacent electrodes and measures differential voltages between other electrode pairs. The system may therefore consist of a single pair of current sources and a single differential amplifier which may be switched between any electrode pairs. Obviously, frequency-difference based back-projection requires operation at more than one frequency.

The other methods require absolute voltage measurements referenced to a single electrode or a common ground, but the current may still be applied to a single pair of electrodes. These absolute voltage values may be constructed from differential voltage measurements. Some groups [65, 71] have preferred to apply trigonometrically based current patterns, requiring multiple current sources with independent amplitude control, but this approach is inappropriate for the back-projection method. If adaptive currents are used then multiple current sources with amplitude control are essential.

CHAPTER THREE
Image Reconstruction Software

3.1 Introduction

EIDORS (Electrical Impedance and Diffuse Optical tomography Reconstruction Software) is a software suite for image reconstruction in electrical impedance tomography (EIT) and diffuse optical tomography (DOT). Its goal is to provide freely distributable and modifiable software for image reconstruction of electrical or diffuse optical data. Such software facilitates research and development in these fields by providing a reference implementation against which new developments can be compared, and by providing a functioning software base from which new ideas may be built and tested. Making the source code available also facilitates scrutiny of algorithms and their implementation by other researchers. The original EIDORS (version 1) software [72] is based on software from the dissertation of Vaukhonen [73]. It implemented a MATLAB package for two-dimensional mesh generation, solving of the forward problem and reconstruction and display of the images. In order to provide capability to solve 3D reconstruction models, a new project, EIDORS3D (version 2), was begun [74], based on the software developed for the dissertation of Polydorides [75] The EIDORS software packages shared the same numerical and algorithmic foundations, but shared very little software code. Each software package modelled the medium under investigation using a simplex based finite element representation, and images were reconstructed using regularized inverse techniques.

In the three years since the publication of EIDORS3D, several patterns of use have been noted. Researchers typically download the software, run the provided demonstration examples, and make modifications in the demonstration examples and the software internals to meet their needs. Because of the lack of a modular software structure of EIDORS3D, changes tended to be made into the code itself. This resulted in duplicated code which could not easily be refactored in order to be contributed back to EIDORS. Additionally, recent work has begun to move away from basic reconstruction algorithms, focussing on such issues as mesh generation, electrode modelling, visualization and electrode error detection. Such research would be facilitated by using modular components which could be plugged" into a selection of reconstruction algorithms.

To address these issues, the EIDORS software has been completely restructured with the goal of providing an extensible software base designed to support community use, modification and contribution. These modifications have been released as EIDORS version 3 (currently at release 3.1), which incorporates the following features:

- *Multiple algorithm support*: EIDORS V.3 has been redesigned to allow flexibility of using multiple algorithms (or parts of algorithms). This version provides access to the algorithms of [76], [77], [74], [78] and [72]. We feel that this capability is becoming more important with a trend toward meta-algorithms in EIT, such as algorithms for detection of electrode errors [79].
- *Generalized model formats*: One limitation of previous versions of the EIDORS software is that they were designed around specific electrode configurations and stimulation and measurements patterns. While it was possible to use the software for more general configurations, this was a fairly daunting task. In order to support the wide variety of EIT measurements and algorithms, EIDORS now provides a general EIT model format (i.e. the **fwd_model** structure). Additionally, several utility functions are provided to create common electrode and stimulation configurations. This format specifies the electrode positions, contact impedances, and stimulation and measurement patterns, and all supported algorithms are able to reconstruct images based on data provided in these formats.
- *Interface software for common EIT systems*: functions are provided (in the interface directory) to load from a variety of EIT hardware storage formats into the EIT data format. Currently, EIDORS will detect when data do not match the specified protocol in the **fwd_model**, but will not (yet) automatically convert the data. At this point it has only been possible for the developers to offer support for EIT hardware that they have access to. We hope that EIDORS will attract contributions from software developers who have access to other hardware systems.
- *Usage examples*: It is observed that researchers typically base new software on demonstration examples. To facilitate this, several simple and more complex usage examples are provided for image reconstruction in two and three dimensions using various image reconstruction algorithms and combinations of algorithms.
- *Test suite*: Software is intrinsically difficult to test. While little work has been done specifically on testing numerical software for inverse problems, we believe that such tests are even more difficult. EIDORS has begun to implement a series of regression test scripts (in the tests directory) to allow automatic testing of code modifications. For example the function

calc_jacobian_test.m validates a function to calculate the Jacobian against an approximation of the Jacobian using the perturbation method.

- *Open-source license*: EIDORS is licensed under the GNU General Public License [80].Users are free to use, modify, and distribute their modifications. All modifications must include the source code, or instructions on how to obtain it. EIDORS may be used in a commercial product, as long as the source code for EIDORS and all modifications to it are made available.
- *Sourceforge hosting*: In order to allow collaborative development, EI-DORS is hosted by sourceforge.net available at http://eidors.org or http://eidors3d.sf.net. Software is available for download as packaged released versions (version 3.1 was released on 24 Jan 2006), or the latest developments may be downloaded from the Concurrent Versions System (CVS) [81]. Sourceforge hosting allows for collaborative development for group members, while permitting read-only access to everyone. In order to become a member of the developer group, new contributors should contact the authors. One concern with a distributed software project is the possibility of conflict due to disparate authors working on the same module. Version control software such as CVS is widely understood to facilitate collaborative development, and manage software version conflicts [81].
- *Language independence*: (Octave and Matlab) EIDORS was originally written for Matlab. However, the eventual goal is to support multiple mathematical software packages. Some progress has been achieved, and EIDORS version 3 works with Octave [82], although some advanced graphics functions still function only with Matlab. The current version of EIDORS works with Octave (version > 2.9.4) and Matlab (version > 6.0). Support for Octave was motivated by two goals: first, octave provides a free software platform which can encourage the development of embedded and commercial applications of EIT which are currently limited by the cost of Matlab, and secondly, Octave provides an open source platform to match the open source nature of EIDORS.
- *Pluggable code base*: In order to facilitate user modifications, EIDORS has been designed to provide some of the benefits of object-oriented (OO) software [83]: abstraction, encapsulation, polymorphism and inheritance. This design uses function pointers to allow adding new modules and controlling which parts of functions are executed. EIDORS is thus able to offer the OO features of packaging and polymorphism, while not encapsulation or inheritance.

- *Automatic matrix caching*: In order to increase performance of image reconstruction software, it is important to save and reuse values of computationally expensive variables, such as the Jacobian and image priors. Such caching complicates the software implementation, and potentially leads to errors. In order to simplify design, EIDORS offers the ability to automatically detect when a calculation requests a value previously calculated, and will automatically retrieve that previous value. EIDORS extracts caching to a separate module **eidors_obj**, in a way that will generally happen transparently for the programmer. This capability helps software based on EIDORS to be more clear and easier to decompose into functional modules.
- *Enhanced Finite Element Modelling and Graphical output*: Image reconstruction, especially in 3D, requires functions to show high quality graphical representations of the images. EIDORS provides several functions for image presentation using the Matlab graphics features, as well as functions to display images using the VTK visualization program [84], after exporting the data to a vtk file. **Show_fem.m** displays a three dimensional model of the finite element mesh and conductivity changes, while **show_slices.m** allows generation of images of arbitrary two dimensional slices through a volume. All EIDORS graphics functions now use a single colour mapping function **calc_colours.m**, which allows global modification of all image colouring using a global variable **eidors_colours**. For modelling, the **create_tank_mesh_ng.m** function is provided to generate a finite element mesh of a cylindrical tank with circular of rectangular electrodes using the netgen [85] mesh generator.

3.2 Software Architecture

This section describes the structure of EIDORS objects and their relationship to the underlying finite element models and numerical functions.

3.2.1 Object Structure

EIDORS software consists of four primary objects: **data, image, fwd_model, inv_model**. Each object is represented by a structure. All objects have the properties of a name and type. The name is arbitrary; it is displayed by the graphics functions, and could also be useful to distinguish objects in a user specified function. The type is used to identify the object type (i.e. data, image etc.).

3.2.2 Forward Model (fwd_model) :

The most complex EIDORS object is the **fwd_model**, which is designed to represent the finite element model (FEM), electrode positions and properties, and stimulation patterns, as well as the pointers to functions to solve the forward problem on this model.

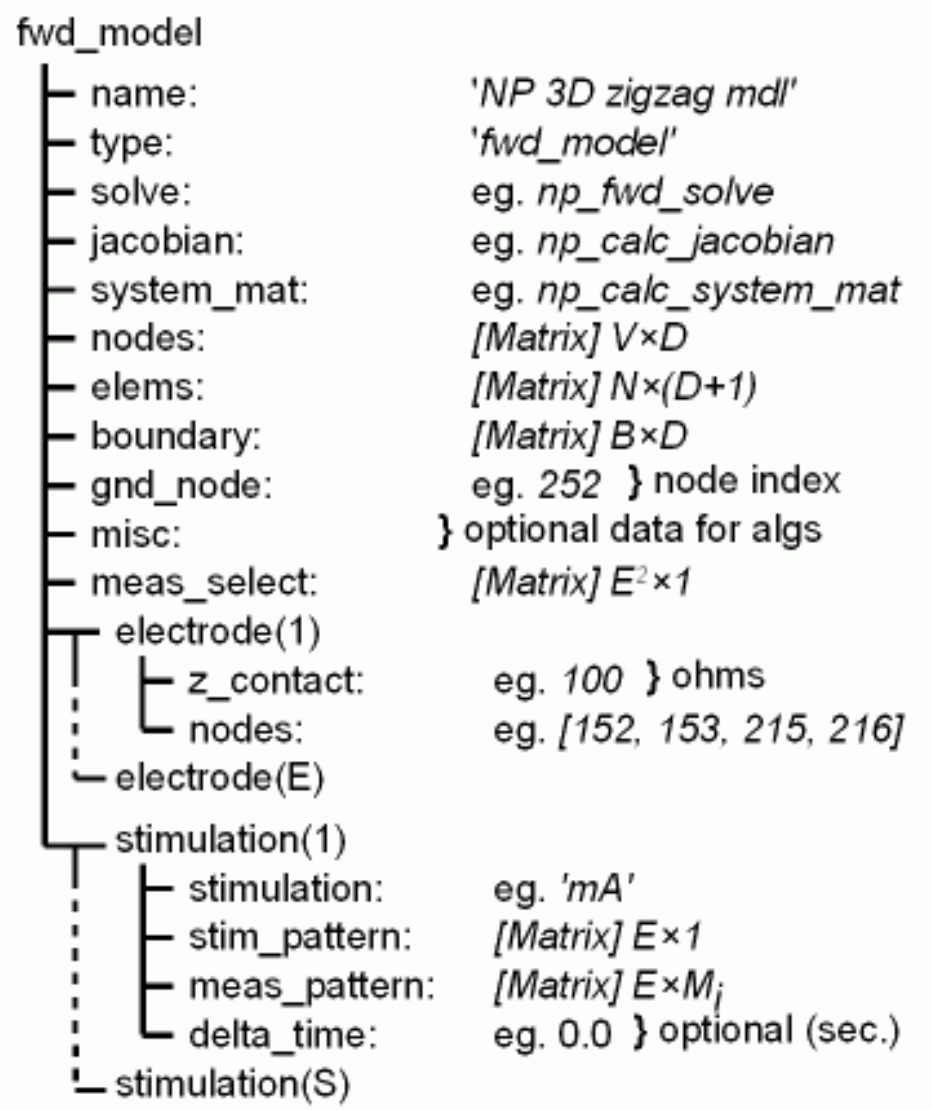

Figure 3.1: The Structure of the EIDORS Forward Model Object.

The FEM is described by the field nodes $(V \times D)$ D), elems $(N \times (D+1))$, and boundary$(B \times D)$, where V is the number of vertices, N is the number of simplices. (And also the number of unknown conductivities to be solved by the inverse solution), B the number of simplices with a face on the boundary, and D the model dimension (D = 2 for 2D and D = 3 for 3D). The ground node is the vertex number attached to ground.

The electrodes are defined by a vector (E × 1) of electrode fields. Each of E electrode objects has fields z_contact (scalar) and nodes (vector) which represent the (possibly complex) contact impedance and vertices to which that electrode is connected. A point electrode would have a single element nodes field with z_contact = 0 while an electrode with a complete electrode model would have multiple vertices specified in nodes and z_contact > 0. Note that EIDORS does not require the electrode model to be the same for all electrodes in a **fwd_model**.

Using these electrodes, sequences of S stimulation patterns are applied and measurements performed in order to generate a frame of data. Stimulation patterns are defined by a vector (S × 1) of stimulation fields. Each stimulation object has fields stimulation, **stim_pattern**, and **meas_pattern**. The stimulation is the quantity stimulated into the electrodes. Typically, EIT systems inject current (represented by "mA"), but the quantity could be voltage (or luminous intensity in an optical tomography system). Currently, EIDORS only accepts current stimulations. **Stim_pattern** is a vector (E × 1) of the stimulation quantity applied to each electrode during that stimulation pattern. Each stimulation object also has an optional **delta_time** field representing the time increment between measurements at this stimulation and the beginning of the measurement frame. Such data may be used to perform Kalman filtering, for example. **Meas_pattern** is a (sparse) matrix ($E \times M_i$) representing the M_i measurement patterns for stimulation i. Each column of this matrix represents the amplification of the signal at each electrode for a single measurement pattern. For example if measurement k = 2 is the difference signal between electrodes 4 and 5, then $\mathbf{meas\_pattern_{j;k}}$ is 1 for j = 4, -1 for j = 5 and zero for other values of j when k = 2. EIDORS does not require that the number of measurement patterns be equal for each stimulation pattern. The total number of measurements per frame is $M = \sum_{i=0}^{S} M_i$

For many EIT systems, an adjacent stimulation pattern is used with no measurement taken at current stimulation electrodes, given $M = E \times (E - 3)$. For a 16 electrode system, this gives 208 measurements (or, considering reciprocity, 104 independent measurements). One practical consideration is that many EIT systems store data as a matrix of size $(E^2 \times F)$ where F is the number of data frames. In this case E^2 = 256 of which $3 \times E$ = 48 measurements in each frame yield zero. In order to allow easy use of EIDORS with such systems, the optional field **meas_select** $(E^2 \times 1)$ is defined for the **fwd_model**. This field

contains a 1 in each position corresponding to a used measurement pattern in the frame (thus **meas_select** will have M ones).

EIDORS provides several utility functions to define the fields of the **fwd_model** for common patterns, such as the **mk_circ_tank.m, mk_stim_patterns.m** and **mk_common_model.m** functions. These functions allow easy definition of circular and cylindrical FEM models with rings of electrodes and adjacent stimulation protocols.

The **fwd_model** contains three function pointers to allow solution of the forward problem, **solve, jacobian** and **system_mat**. Each field contains the function name (as a string) or a function pointer to calculate these quantities. In each case, these quantities are solved using the utility functions **fwd_solve()**, **calc_jacobian()** and **calc_system mat()**. For example, given a **fwd_model** object **fmdl**, we may calculate the system matrix, **Smat**, using:

Smat = calc_system_mat(fmdl);

This code will call the appropriate function and also manage the caching of the computed result. In this case, if a system matrix has previously been computed for a **fwd_model** object with the same values as **fmdl**, then the previous result will be returned, without the computation function being called.

3.2.3 Data

An EIDORS data object represents a frame of measurement or simulated data. The required fields are the actual frame data, **meas**, and the acquisition time, **time**, in seconds after the epoch. In a particular application time may be defined with respect to another start point, such as the start of the experiment, or may be set to 0 or -1 for unknown times or simulated data.

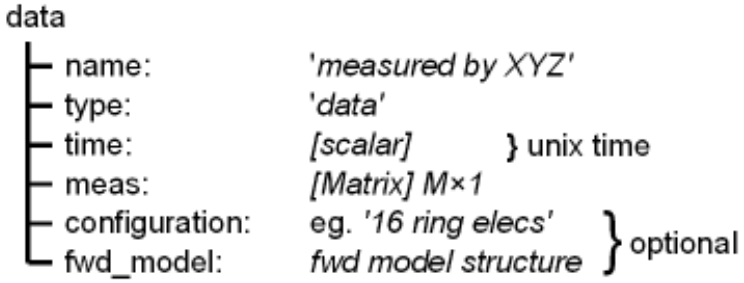

Figure 3.2: The structure of the EIDORS Data Object.

The **meas** field is a $M \times 1$ matrix where M is the number of measurements in each data frame (the sum of number of measurements for each stimulation pattern). The data in **meas** is ordered such that the measurements for **stimulation(1)** are first.

Data may be loaded into EIDORS using the **eidors_readdata()** function, which provides an interface to the storage formats used by some EIT equipment manufacturers. The data object may also contain two options fields, configuration and **fwd_model**. Specification of **fwd_model** allows EIDORS to validate that the data are being interpreted correctly, and being reconstructed using the correct model. The configuration is a user specified string with a similar function; software may assign a value to this field in order to distinguish data objects.

3.2.4 Inverse Model (inv_model)

The **inv_model** object groups information necessary to allow reconstruction of images. Two basic types of reconstruction are distinguished based on the **reconst_type** field, “difference" (which calculates an image based on the difference between two data objects) and “static" (which calculates an image based on a single data object).

The pointer to the solver function is stored as a string or function pointer in the **solve** field. The provided functions are based on regularized image reconstruction algorithms, and require an image prior and a choice of hyperparameter. The latter is specified in the **hyperparameter** field. For simple cases, a scalar value is provided in the **value** field. However, for more complex cases, a hyperparameter selection strategy is specified as a function in the **func** field. One example is the noise figure strategy of [76]. This strategy may be specified by setting **hyperparameter.func='aa_calc_noise_figure'** and **hyperparameter.noise.figure=Value.**

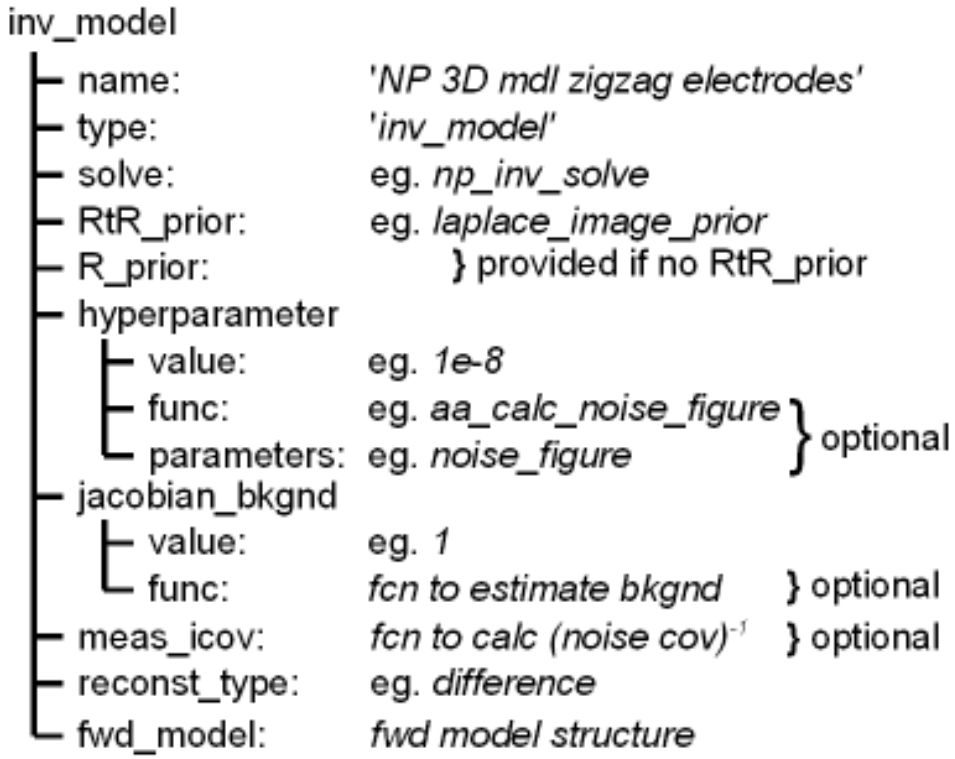

Figure3.3: The Structure of the EIDORS Inverse Model Object.

Image priors are commonly used in two ways, using either a regularization term of $||\lambda Rx||$ or $||\lambda x||_R$, where **x** is the vector of image element values. In the most common case, a quadratic norm is used, and these regularization terms may be expressed as ¸$\lambda^2 x^t Rx$ or ¸$\lambda^2 x^t R^t Rx$, respectively. One implementation concern is to make it clear to the user which type of image prior is required. EIDORS addresses this by defining two different functions to calculate image priors**, R_prior** and **RtR_prior**. A user may provide a value for either or both. When the algorithm specified in the **solve** field is called, it will request either an **R_prior** or **RtR_prior**. If the **RtR_prior** is required, but the **R_prior** is specified, then it will be calculated from R^tR. Similarly, EIDORS will attempt to calculate **R** from the Cholesky factorization of the **RtR_prior**, if required. Parameters to an image prior function are specified in a field, using the name of the mage prior function, added to the **inv_model** object.

3.2.5 Image

The EIDORS image object expresses the reconstructed or simulated conductivity values. The field ***elem_data*** $(N \times 1)$ *is the value of each of the image* elements in the finite element model (in the field **fwd_model**).

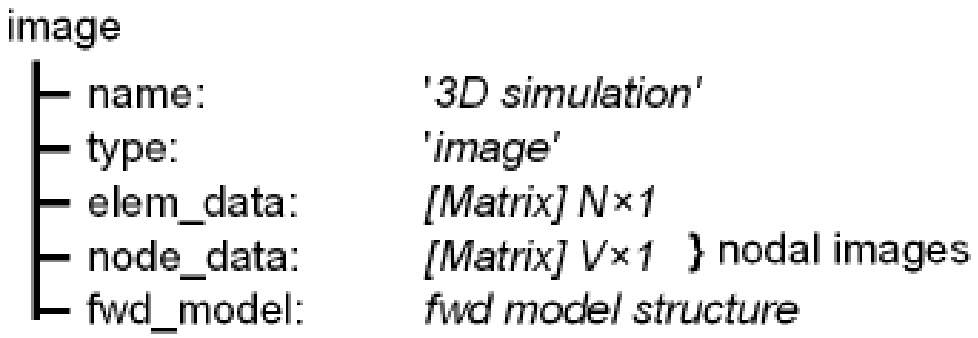

Figure 3 4: The structure of the EIDORS Image Object.

For example, given an **inv_model** object **imdl**, we may express image reconstruction by (assuming difference EIT, and data objects data1 and data2):

```
img= inv_solve( imdl, data1, data2 );
```

Similarly, in order to simulate data object **datasim** from a simulation image **imgsim**, we may write:

```
datasim = fwd_solve(fmdl, imgsim);
```

Start		
	Create electrode model	%%Create simple 16 electrode finite element model of core and electrodes with homogeneous resistance
	Solve forward problem	%% solve for voltage distribution with electrode model
	Load	%%Load real voltage measurements
	Create Inverse electrode model	%%Solve for resistivity distribution using the invers electrode mode, forward voltage measurements, and the real voltage measurements.
	Display	%%Display the final resistivity distribution image
End		

Figure 3.5: Simplified Code Structure for EIDORS MATLAB Data Processing Program

3.3 EIT Processing

The processing of the EIT voltage data was accomplished using the EIDORS toolkit for MATLAB. Shown below in Figure 3.5 is a simplified code structure for the data processing. The first step in solving for the internal resistance distribution was to create a finite element model of the core and electrodes, Figure 3.6. With this finite element model and a set current, the forward problem was solved assuming a system of homogeneous resistance for the voltage data.

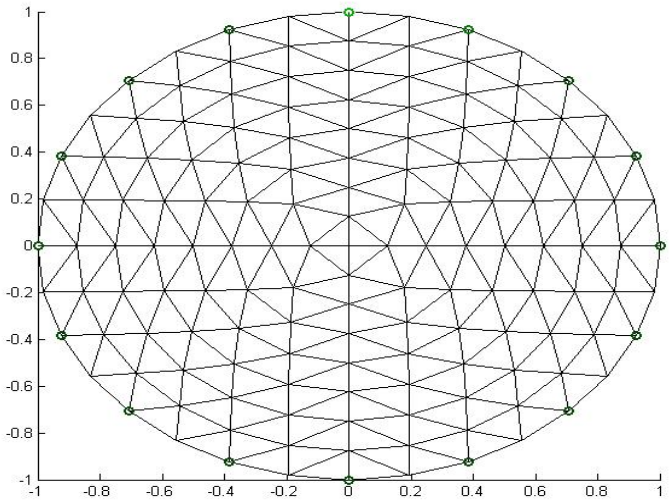

Figure 3.6: Finite Element Mesh and Electrodes used to Solve Forward Problem

The next step was to load the real data set and solve the inverse problem. The inverse problem was solved using the different methods, which the EIDORS toolkit offers and other regularized nonlinear solvers to obtain a unique and stable inverse solution. After solving for the resistivity distribution the final image is reconstructed and displayed

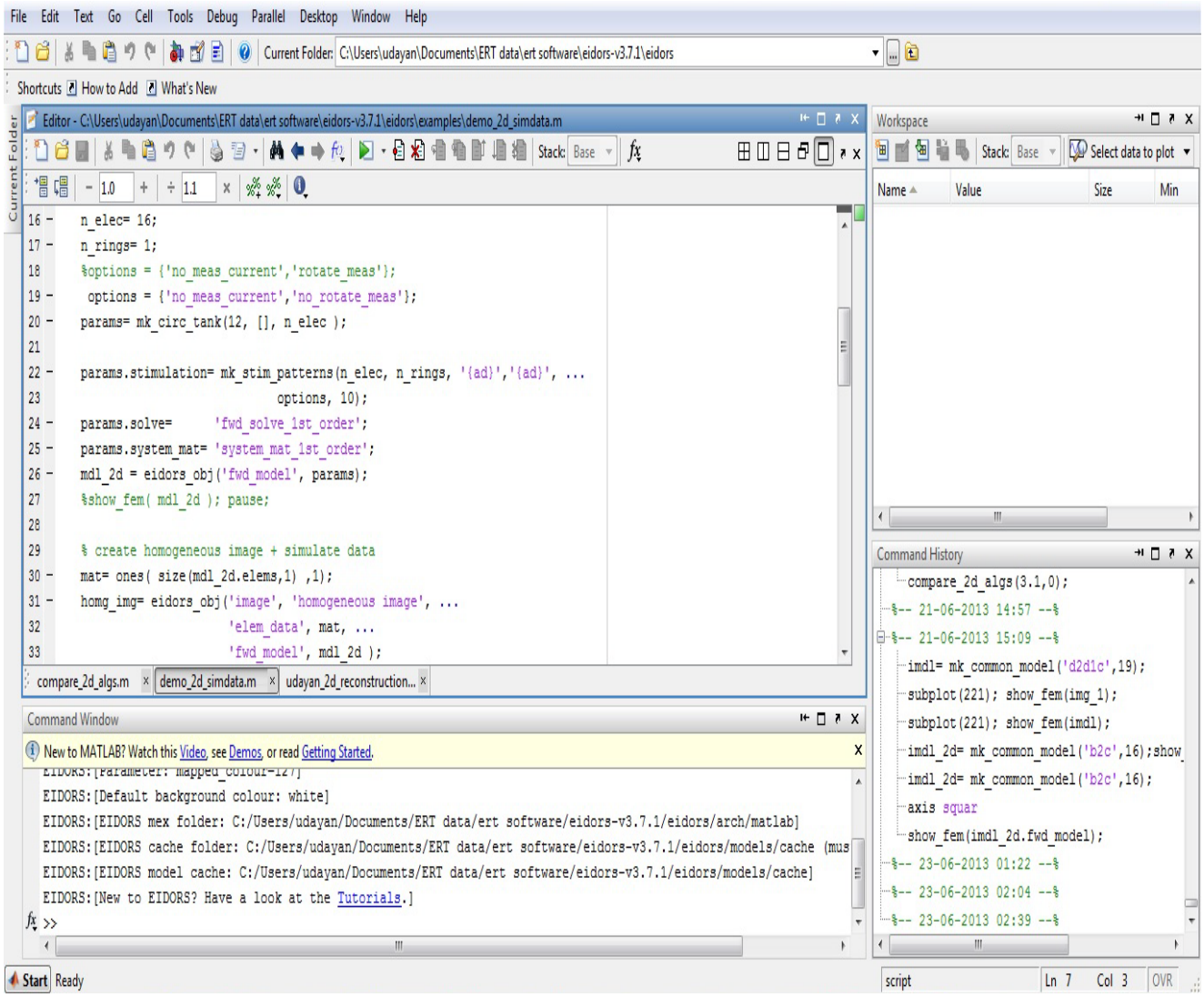

Figure 3.7: Screen-shot of the EIDORS-toolkit on the MATLAB

4.1 System Design

The overall system comprises of three elements (see figure 4.1). Tomography controller, Data Acquisition system and Reconstruction software. The system is controlled by the Tomography Controller (combination of hardware and software), which calls on and passes data between the Data Acquisition system and the Reconstruction Program. These are briefly described in the following sections. The block diagram of the whole system is shown in figure 4.2 and the real photo of real system is shown in figure 4.6

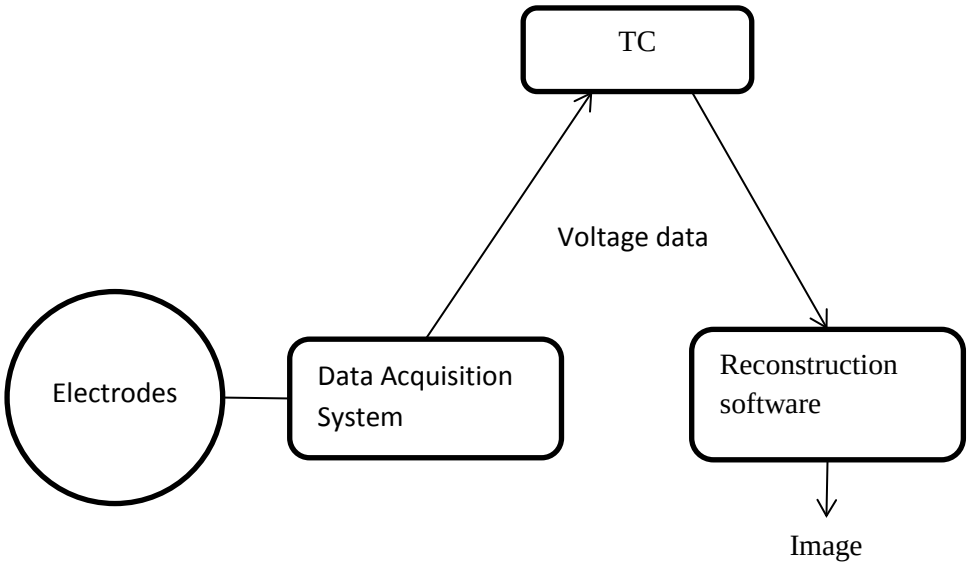

Figure 4.1: Block Diagram of EIT System Process

4.2 Tomography Controller

The Tomography Controller is 8051 microcontroller based control system which is used co-ordinates the operations of the Data Acquisition System and the Reconstruction algorithm. It is the roll of the TC to switch between electrodes during scan cycles. When following the adjacent current patterns first the adjacent electrodes for e.g. electrode 1 and 2 are driving pair so electrode 1 is connected to the constant current source generator and the electrode 2 is connect to the common ground and the differential voltage is measured one by one between

electrode 3-4 then 4-5 and so on till 15-16. Then then driving pair is change and same procedure is repeated.

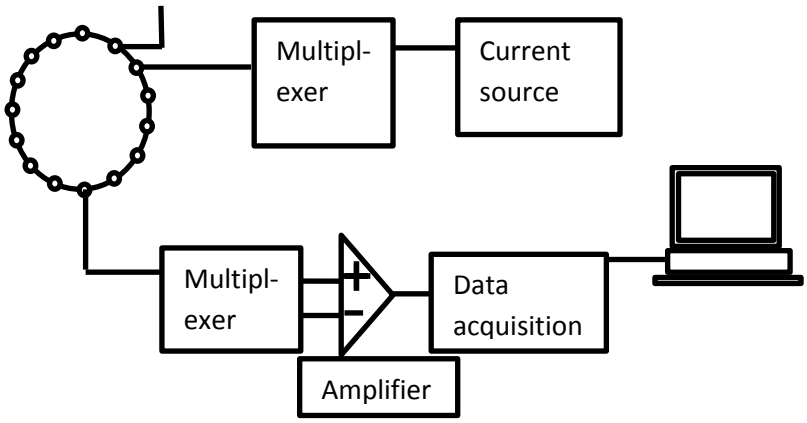

Figure 4.2: Typical Imaging System with 16 Electrodes attached to the Boundary of an Object for Current Injection and Voltage Measurement

The main part of the TC circuit is the 8-bit microcontroller (AT89S51) and the multiplexer (HCF4051) used for high speed switching and making connection of electrodes to ADC and the constant current source. The final part is the serial communication (RS232) for the communication between the TC and the computer. The baud rate of 9600 is selected to send the data to computer. The circuit diagram of the TC is shown in the figure

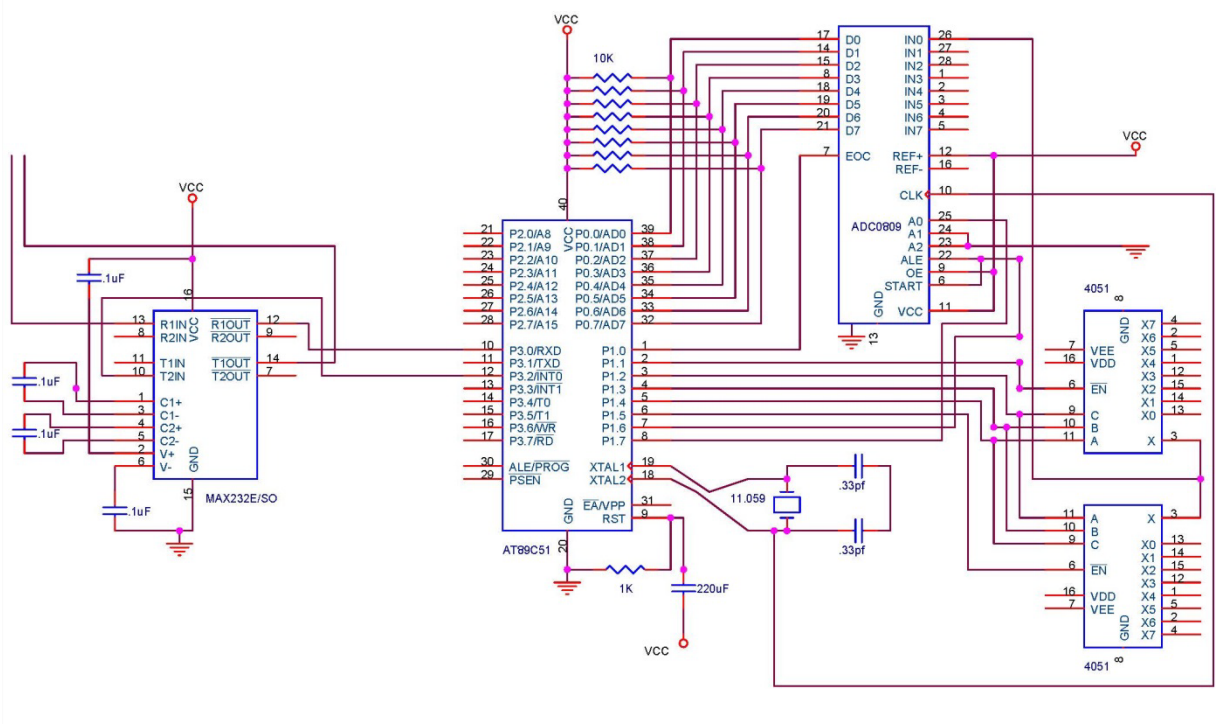

Figure 4.3: Block Diagram of the Data Acquisition System Designed on ORCAD Software

The TC provides the user to change the current patterns and sampling time by changing the program in the Microcontroller. The software for controller and data acquisition units was developed in the assembly language of microcontroller 8051. The acquired data was serially communicated to the Visual Basic 10.0 platform based program this user friendly VB software allows one to select the name and location of the output data file

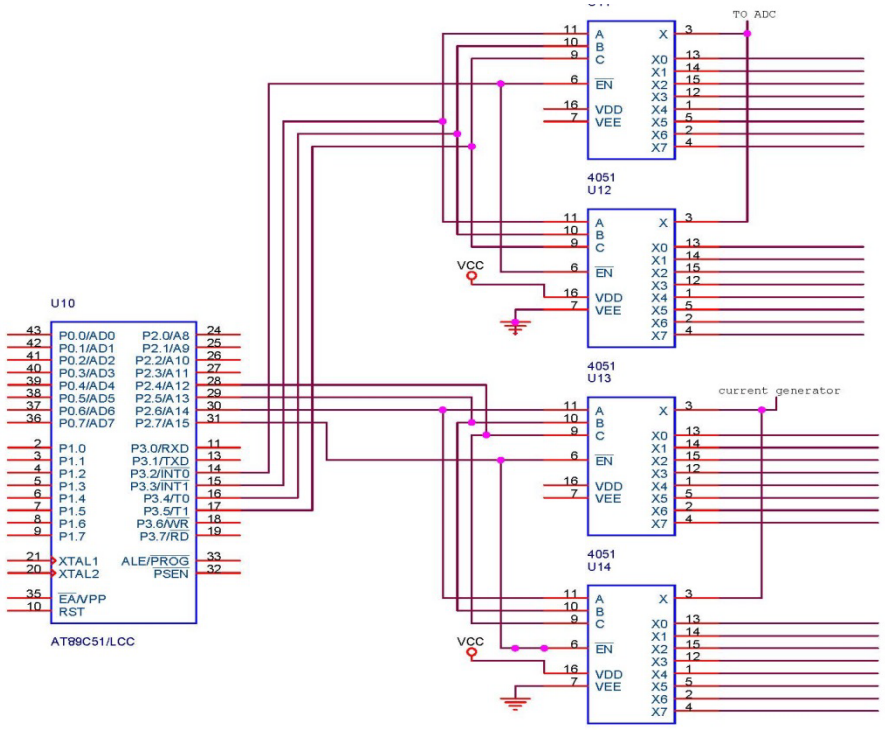

Figure 4.4: Block Diagram of the Tomography Controller. Designed on ORCAD Software

4.3 Current Application System

The data acquisition system must apply current at controllable amplitudes. As the sum of current applied must equal zero, according to Kirchhoff's current law. For the system to be able to apply current to any electrode, other electrode has to sink the current.

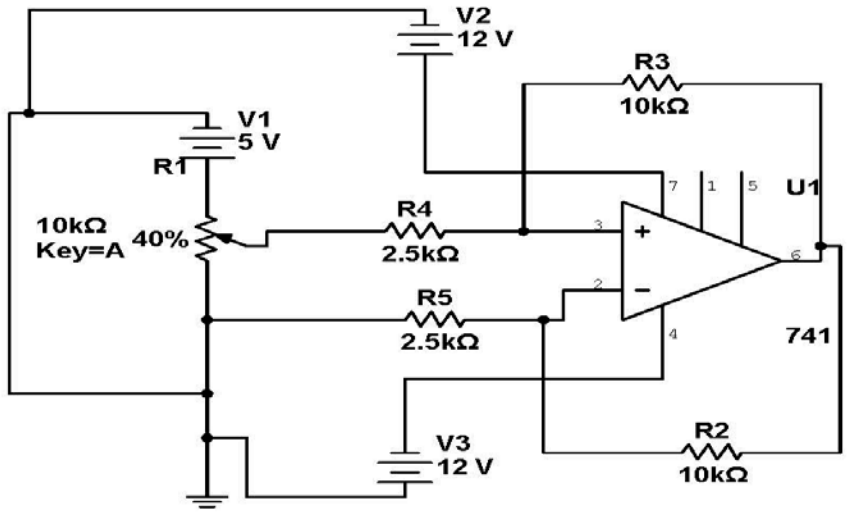

Figure 4.5: Circuit Diagram of Constant Current Source made on multisim11 Software.

Two solution to this problem is possible, either a 17th electrode is connected to the observed region with relatively low impedance to the ground of the data acquisition system, or one of the existing 16 electrode is grounded by a low impedance instead of being left open. In the second case, the current flowing through the grounded electrode will be close to intended current if the source is applying current which is close to the correct current. The first solution is better in terms of symmetry because the current errors will be of similar magnitude for all 16 electrodes. While the second approach is less accurate, but this approach did not appear to produce any problem in the reconstructed images as such and is easy to employ and so this method was used.

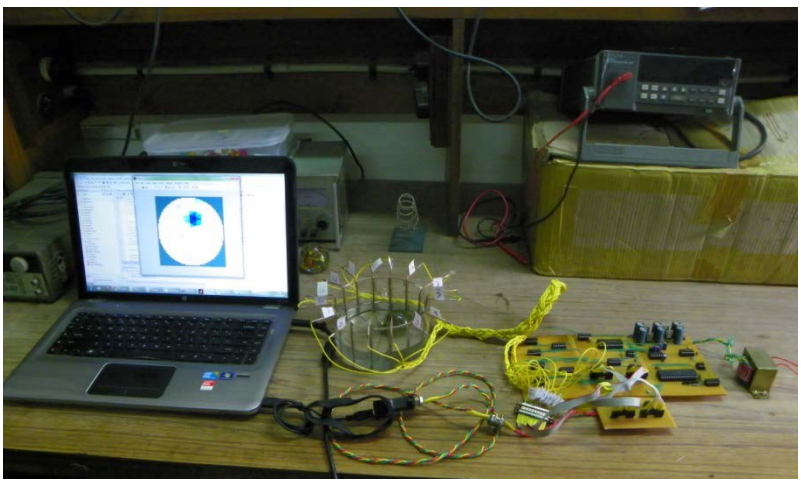

Figure 4.6: Photograph of the Rear System.

The constant current source is generated using an operational amplifier (OP-07) circuit shown in figure.4.5. The current source generates a 1 milliamp current. The circuit is stable and provide constant current even at very high loads, which is the necessity for the EIT system. The output of this is directed to each of the 16 electrodes using the multiplexers which are controlled by the TC.

4.4 Data Acquisition System

The data acquisition system is required to apply current and measure voltages under the control of the TC. As the system is intended for the adjacent current pattern tomography, this implies the need for just one single constant current source. The system is designed to use the single current source which is applied to each electrodes turn by turn by using the multiplexers to connect the source to one particular electrode at a time. The switching is done very quickly and there is not much noise or interconnect problem between channels due to switching.

The main part of the DAQ is the 8-bit resolution analog to digital converter (ADC 0809) with conversion time of 100 microseconds. One per amplifier is also connect before the ADC the key features of the ADC IC is as follows

- Easy interface to all microprocessors
- No zero or full-scale adjust required
- 0V to VCC input range
- Outputs meet TTL voltage level specifications

As using common channels for applying the current and measuring the voltages, only need the 16 channels for 16 electrodes, which make the system less complex and less prone to the measurement errors. The block diagram of the data acquisition system is shown in figure 4.3.

The speed of the system is constrained by the speed at which voltage data can be measured from the electrodes. In order to achieve high speed data acquisition, one of two approaches may be adopted. Either the voltage data is taken in parallel, in which case relatively slow ADC's may be employed, or data is taken in series using a single fast ADC and a fast multiplexer. The single-multiplexed ADC was the less expensive solution and so this

approach formed the basis of the data acquisition system. Consequently, the data acquisition system must include an analogue multiplexer and a fast ADC.

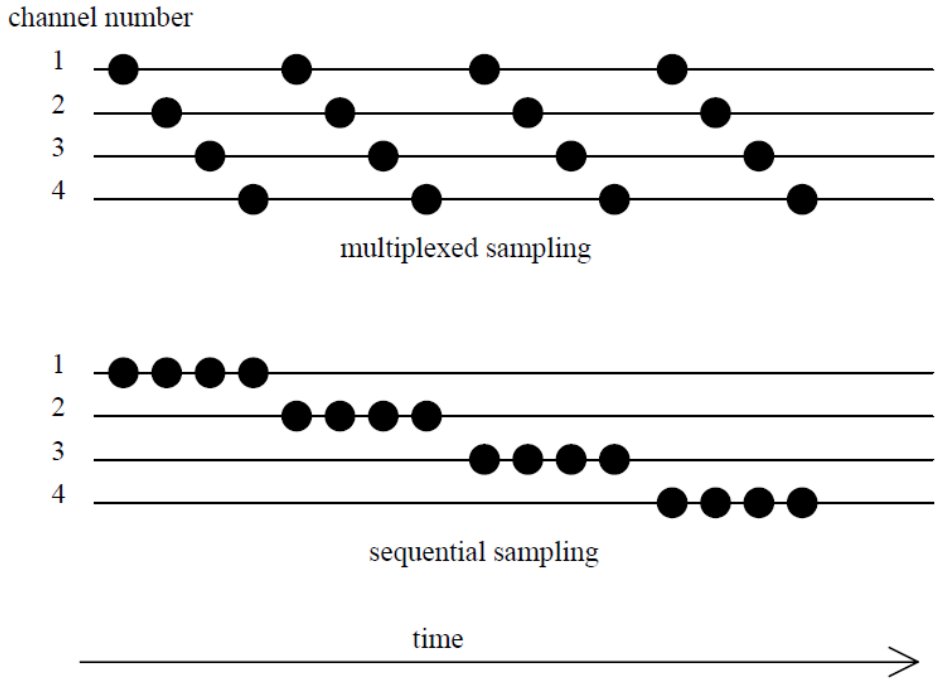

Figure 4.7: Illustration of Multiplexed and Sequential Sampling

A number of possible data collection strategies are possible. Simple examples of two such approaches are shown in figure 4.7, assuming just four channels and four samples per channels for simplicity. The first method illustrated, termed “multiplexed sampling”, requires the system to take one sample on one channel and immediately switch to the next channel for next sample. This leads to a narrow bandwidth because the samples on any one channel are taken over a long period T and bandwidth of the system between the first zero-crossing is 2/T. The second approach, termed “sequential sampling”, involves taking a full set of samples on one channel before switching to the next channel, with a wider consequent bandwidth but with image response which occurs at higher frequencies. The first approach may have benefits in terms of reduced noise if the input noise bandwidth is less than 1/T but requires a higher specification in terms of multiplexer switching speed and setting time.

The total number of switching operation per set of 16 v measurements depends on the sampling protocol. The multiplexer must be switched 16 times, with multiplexing sampling and N measurements per channel, the multiplexer must be switched 16N times.

The number of data sets per image is determined by the reconstruction algorithm. Most EIT systems use the maximum number of independent measurements to increase the resolution to maximum. In present system the adjacent current pattern is used in which 13 voltage measurement are required per electrode pair and 16 electrodes are present so for one frame total 208 measurements are done out of which 104 are repetitive.

The HFC4051 are eight channels multiplexer selected for high-speed channel switching with just 20 nanoseconds settling time. This is connected to the A high speed 8-bit ADC card (ADC0809) which can convert at a rate of up to 1280Khz. 100µs must therefore be allowed for conversion. If the system is driven by 1280KHz clock to match the maximum conversion rate of the ADC, then the timing resolution is 100µs. 300µs must therefore be allowed for multiplexer switching the maximum interval between successive conversion is therefore 100µs +300 µs = 400 µs.

It was decided that the control of the multiplexer switching and the timing of the ADC measurements should be controlled by software rather than hardware to allow a number of different sampling protocols to be applied. The sequence and timing of the measurements is therefore controlled by microcontroller. The block diagram of the DAQ is shown in figure4.3.

4.5 Absolute or Differential Measurement

The majority of EIT systems at present utilise differential voltage measurements. One reason behind this is that such systems use reconstruction based on the back-projection method, a method which uses differential voltages directly. A second advantage is the relative noise immunity of differential measurement in comparison to single-ended measurement with respect to ground. This is because the pair of electrical connections to adjacent electrodes may be physically close together and hence capacitive coupling from a relatively distant voltage source will produce common-mode rather than differential-mode induced signals. The common-mode rejection of the differential-to-single ended conversion will help to reduce the induced noise. However, this effect can only be effective if the electrode impedances involved are similar in value, and electrode guarding may remove the advantage.

Reconstruction methods not based on back-projection often use absolute voltages for reconstruction [20, 21]. These values may be obtained from single ended measurements or from the summation of adjacent differential voltage measurements with one electrode defined

with respect to ground (for example assumed to be 0V). In this case, the use of differential measurements implies smaller voltage values to be measured than the single-ended case and therefore, after amplification by a programmable gain amplifier, a consequent reduction in quantisation error. On the other hand, the summation of differential voltages, as just described, will result in the summation of a number of errors due to input noise and hence will tend to degrade the accuracy of the final value, compared with a single measurement.

4.6 Reconstruction

The reconstruction is done by the software called EIDORS which Provide free software algorithms for forward and inverse modelling for Electrical Impedance Tomography (EIT) in medical and industrial settings. Many reconstruction algorithms are available for use like back-projection method, Newton's method, GREIT (Graz consensus Reconstruction algorithm for EIT) [86]. More detailed description is given in the chapter 3 of this dissertation work.

The following specifications have been defined for GREIT:

• Single ring electrode configurations with Sheffield-type EIT systems, using adjacent current injection and measurement.

• Linear (i.e. real-time) reconstruction of a 2D conductivity change image, based on a 3D forward model.

• Quantitative difference reconstructions for which units can be assigned to EIT images.

• Reconstruction onto a 32×32 pixel array for a single ring of 16, 12 and 8 electrodes, for the shapes: a) neonatal chest, b) male and female adult chest, and c) cylindrical tank.

To run the EIDORS software package on computer we required MATLAB (≥7.0) or Octave (≥3.6), Netgen Mesher (optional) required if we want to generate customized meshes. The software is very flexible and provides many regularization algorithms to improve the quality of the final solution. The software also provides wide variety of hyperparameter selection which is very crucial when solving the inverse problems. More detailed description of the software is discussed in Chapter 3.of this Dissertation.

5.1 Results

The system is tested on the test phantom; the test phantom consists of a 15cm diameter beaker as show in the figure 5.1, 16 cupper electrodes are mounted on it with the help of the industrial glue. The same electrodes are used for the current injection and voltage measurement, the electrode are equally-spaced around the interior of the beaker. All the electrodes are of equal height as that of beaker (10cm). The adjacent current pattern is applied and total 208 voltage readings are taken for making one frame after taking the data zeros are added at the place of driving electrodes in the data sets. And the final data set is made to 256 data points to meet the software requirement. All the reconstructed images are in 2D and of "difference" type.

Figure 5.1: Left Image Showing the Top View and the Right Image Showing the Side View of the Phantom

A standard set of configuration was devised for use in different operating conditions. These are summarised below

A: First a reference run was conducted in which the tap water is used which is filled in the beaker up to the height of the 2.5cm.

B: second a non-conducting object (glass paper weight) is placed on the co-ordinates (2,2). inside the beaker and almost equal amount of water which is displaced by the object is taken out of the beaker, then waited for 5 more minutes to settle the water then measurements are taken.

The images are presented in the figures 5.1 and figure 5.2 the images are reconstructed using one step inverse solver using Diff GN one step method and Laplace for making regularization matrix. The reconstructed images are affected by a factor used during reconstruction called the Tikhonov factor. Each of these images was obtained using a Tikhonov factor of 0.2, a value which was found to produce good images.

The results show that Difference and absolute both type of imaging is possible with the system. Conducting and insulating objects are imaged close to their true locations.

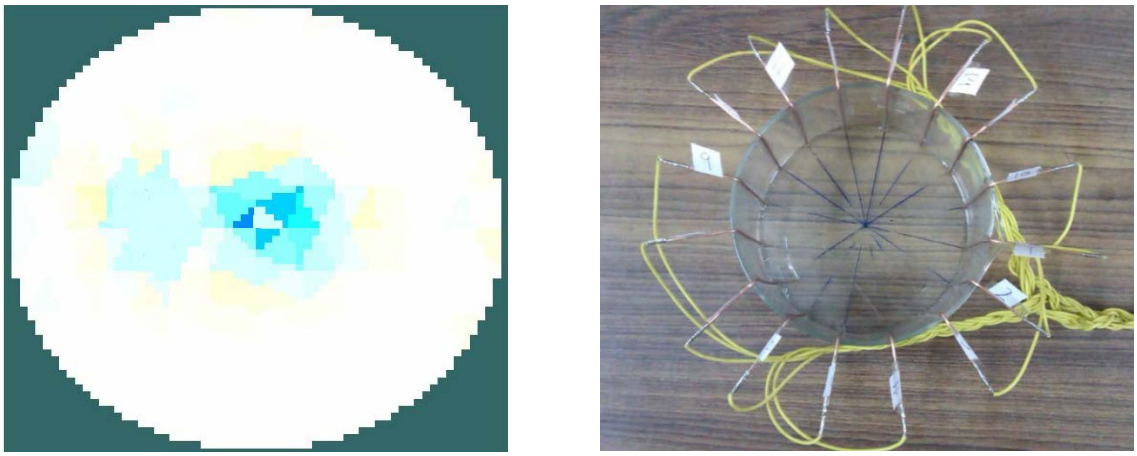

A B

Figure 5.2: A Reconstructed Image of the Reference Top Water in Beaker B: Real Photo of the Beaker Filled with Tab Water

As it can be seen in figure 5.2 that at the centre the noise signal are generated while nothing is present at the centre but still the artefacts can be seen clearly in the reconstructed image the spatial resolution for reconstructed image depends on the different current patterns we can apply and measure the voltage readings and in this case we are only using 16 electrode and one current pattern that's why the centre part is not very clearly reconstructed.

A B

Figure 5.3: A Reconstructed Image of the Test Phantom. B Real photo of the test phantom.

In the figure 5.3 it can be seen that the reconstructed images are exact replica of the real object although the shape of the object is not very clearly reconstructed but the object can be detected in the reconstructed image.

	Laplace	TV	Gaussian HPF
Diff GN one step	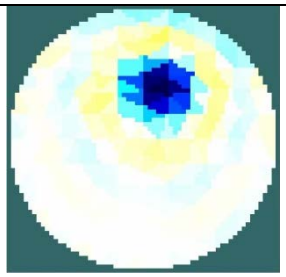 1	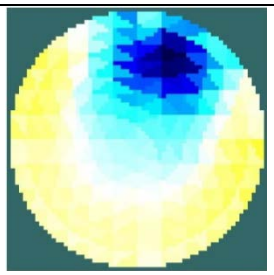 2	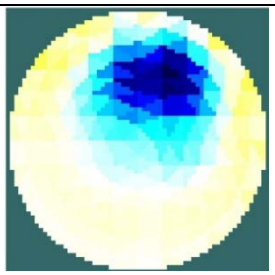 3
TV Pdipm	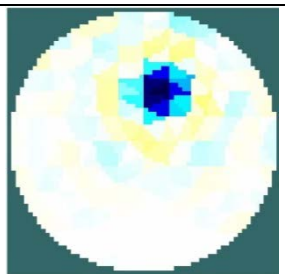 4	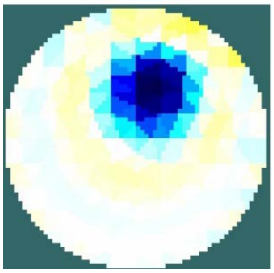 5	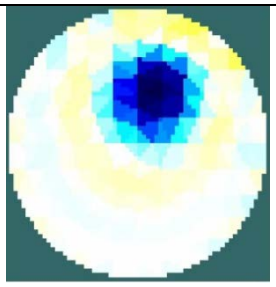 6
TV Irls	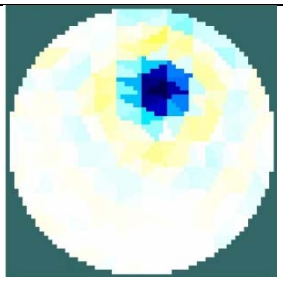 7	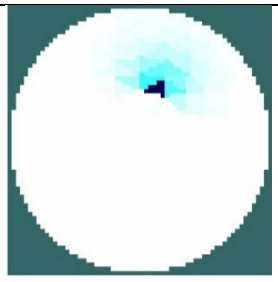 8	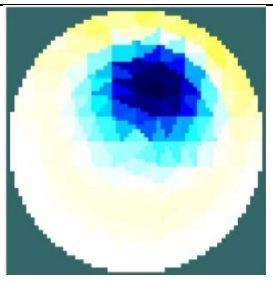 9

Figure 5.4: Reconstructed Images using Different EIT Techniques

top left corner the 1st image is one step inverse solver using approach of Adler&Guardo 1996 method (Diff GN one step) for inverse solution with Laplace image prior; 2nd image is one step inverse solver using approach of Adler&Guardo 1996 method (Diff GN one step) for inverse solution with Total variation as image prior; 3rd image is one step inverse solver using approach of Adler&Guardo 1996 method (Diff GN one step) for inverse solution with

Gaussian High pass filter (Gaussian HPF); 4th in the row was Total Variation inverse solver for absolute data using Primal/Dual interior point method (TV Pdipm) with Laplace for image prior ; 5th image is Total Variation inverse solver for absolute data using Primal/Dual interior point method for inverse solution with total variation method as image prior; 6th Total Variation inverse solver for absolute data using Primal/Dual interior point method (TV Pdipm) with Gaussian for image prior; 7th is Total Variation method with iteratively reweighted least squares for inverse solution (TV Irls) Laplace image prior; 8th is Total Variation method with iteratively reweighted least squares for inverse solution (TV Irls) with Total variation image prior. 9th image is Total Variation method with iteratively reweighted least squares for inverse solution and Gauss-Newton Reconstruction with Gaussian HPF making regularization matrix. All the images are made with hyper-parameter equal to 3e-3.

In order to find which inverse solver algorithm generate best quality images we have used three different inverse solver

- Diff GN one step.
- Total Variation inverse solver for absolute data using Primal/Dual interior point method (TV_pdipm).
- Total Variation method with iteratively reweighted least squares for inverse solution (TV_irls).

And the different regularization methods are also used to further refine the final reconstructed images the regularization methods employ are as follows

- Laplace,
- Total Variation.
- Gaussian High Pass Filter.

The reconstructed images are shown in figure 5.4. And we have also calculated the time consumed by the different algorithms main functions to compare the computation time for different time which is given in the table 1 to 9. And the comparison is given in the Table 1.

When the inverse solver algorithm of Diff GN one step is applied with different image prior algorithms it is found that the least total time was taken by Laplace approach. If self timer is compared it was found that TV and Gaussian HPF are comparable but TV still gives advantage of 0.003 seconds in total time. This inverse approach with Laplace prior approach gives lowest total time amongst all the nine combination used.

The inverse solver algorithm of TV pdipm when used with different image prior algorithms gives similar results for total time. However, image prior algorithm of TV gives higher self timer as compared to other two algorithms used. It was also observed that the total time obtained was maximum for TV pdipm algorithm for all three image prior algorithms.

The TV irls algorithm for image solver gives highest self timer when used with Laplace image prior algorithm. This inverse solver approach also gives higher self timer for all the image prior techniques as the overhead computational requirement is more. However, this algorithm of image solver when used with image prior TV approach gives lowest total time.

Table 1: Comparison of EIT techniques
(All data in secs)

Image Prior / Inverse Solver	Laplace		TV		Gaussian HPF	
	Total Time	Self Timer	Total Time	Self Timer	Total Time	Self Timer
Diff GN one step	0.217	0.003	0.588	0.010	0.591	0.010
TV Pdipm	0.680	0.010	0.830	0.030	0.969	0.010
TV Irls	0.301	0.140	0.230	0.080	0.631	0.090

Table 2: Time Taken by Different Functions for Image 1			
Function name	Calls	Total time (s)	Self timer (s)
inv_solve	1	0.252	0.021
inv_solve_diff_GN_one_step	1	0.217	0.003
fwd_solve	2	0.385	0.015
calc_system_mat	3	0.214	0.003
show_slices	1	0.500	0.042
calc_RtR_prior	1	0.050	0.003

The image one is made using diff GN one step inverse solver method with Laplace as image prior the time for calculating the inverse solver in this case is 0.217 seconds and image prior is 0.050 seconds which means this method is fastest among the other method because this method needed less computation. As shown in the Table 2.

Table 3: Time Taken by Different Functions for Image 2			
Function name	Calls	Total time (s)	Self timer (s)
inv_solve	1	0.720	0.030
inv_solve_TV_pdipm	1	0.680	0.010
fwd_solve	2	0.550	0.030
calc_system_mat	3	0.280	0.020
show_slices	1	0.590	0.050
calc_R_prior	1	0.080	-0.000

The Table 3 is made using Total Variation inverse solver for absolute data using Primal/Dual interior point method and Laplace for image prior the time consumed in this case is 0.680 which is more as compared to the previous but is not the maximum and the image prior is taken 0.080. The forward solver took more time and inverse solver is quit time consuming.

Table 4: Time Taken by Different Functions for Image 3			
Function name	Calls	Total time (s)	Self timer (s)
inv_solve	1	0.470	0.170
inv_solve_TV_irls	1	0.301	0.140
fwd_solve	2	0.361	0.020
calc_system_mat	3	0.180	0.010
show_slices	1	0.441	0.060
calc_R_prior	1	0.060	0.000

As seen in Table 4 when Total Variation method with iteratively reweighted least squares for inverse solution and Laplace, forward solution took 0.361 seconds which is low as compared to other methods mention here the inverse solver also taken less time just 0.470 seconds.

Table 5: Time Taken by Different Functions for Image 4			
Function name	Calls	Total time (s)	Self timer (s)
inv_solve	1	0.668	0.070
inv_solve_diff_GN_one_step	1	0.588	0.010
fwd_solve	2	0.359	0.020
calc_system_mat	3	0.199	0.010
show_slices	1	0.488	0.040
calc_RtR_prior	1	0.239	0.080

Image 4 was made using image is Total Variation inverse solver for absolute data using Primal/Dual interior point method for inverse solution with total variation method for image prior. Forward and Inverse solver took 0.369 and 0.668 seconds respectively for computation.as shown in Table 5.

Table 6: Time Taken by Different Functions for Image 5			
Function name	Calls	Total time (s)	Self timer (s)
inv_solve	1	0.860	0.010
inv_solve_TV_pdipm	1	0.830	0.030
fwd_solve	2	0.520	0.010
calc_system_mat	3	0.270	0.020
show_slices	1	0.560	0.040
calc_R_prior	1	0.050	-0.000

The Table 6 is made from the image 5 computation data. The image is reconstructed using Variation inverse solver for absolute data using Primal/Dual interior point method for inverse solution and total variation method for image prior. The second highest 0.860 seconds was shown by this method in inverse solving.

Table 7: Time Taken by Different Functions for Image 6			
Function name	Calls	Total time (s)	Self timer (s)
inv_solve	1	0.270	0.030
inv_solve_TV_irls	1	0.230	0.080
fwd_solve	2	0.350	0.010
calc_system_mat	3	0.180	0.030
show_slices	1	0.460	0.030
calc_R_prior	1	0.040	0.000

Table 7 shows Total Variation inverse solver for absolute data using Primal/Dual interior point method with total variation method for image prior this method performed very well in computation time but image quality was very poor this method took only 0.270 seconds for inverse solver which is second lowest time consumed.

Table 8: Time Taken by Different Functions for Image 7			
Function name	Calls	Total time (s)	Self timer (s)
inv_solve	1	0.621	0.010
inv_solve_diff_GN_one_step	1	0.591	0.010
fwd_solve	2	0.360	0.010
calc_system_mat	3	0.210	0.010
show_slices	1	0.481	0.040
calc_RtR_prior	1	0.400	0.000

The Image is reconstructed with Total Variation method with iteratively reweighted least squares for inverse solution with Laplace image prior the image quality is considered best by using this method and the time consumed is 0.621 seconds and forward solver it was 0.360 which was below average of time consumed by different methods here. And the computation time is presented in Table 8.

Table 9: Time Taken by Different Functions for Image 8			
Function name	Calls	Total time (s)	Self timer (s)
inv_solve	1	0.999	0.020
inv_solve_TV_pdipm	1	0.969	0.010
fwd_solve	2	0.410	0.010
calc_system_mat	3	0.200	0.020
show_slices	1	0.490	0.030
calc_R_prior	1	0.410	0.000

Total Variation method with iteratively reweighted least squares for inverse solution with total variation image prior method was used in this case which has given poorest image quality as the noise the image features are also degraded the time consume are also maximum 0.999 for inverse solver and 0.410 for forward solver.as shown in Table 9.

Table 10: Time Taken by Different Functions for Image 9			
Function name	Calls	Total time (s)	Self timer (s)
inv_solve	1	0.671	0.040
inv_solve_TV_irls	1	0.631	0.090
fwd_solve	2	0.360	0.020
calc_system_mat	3	0.180	0.020
show_slices	1	0.430	0.030
calc_R_prior	1	0.430	0.030

The Table 10 shows the computation time required by the image is Total Variation method with iteratively reweighted least squares for inverse solution and Gauss-Newton Reconstruction with Gaussian HPF making regularization matrix. All the images are made with hyper-parameter equal to 3e-3.

5.2 Conclusion

A cost effective novel EIT system was developed around 89C51 and used to generate EIT data. The data acquisition hardware (chapter 4) was designed which was capable of high speed switching's between different channels for data acquisition. It also incorporating the constant current source capable of providing the constant current of 1 mA required by the EIT system and voltage measuring circuitry. Design met the requirements needed for implementing the different current patterns like opposite, adjacent current patterns in the basic EIT system. The current work was done using adjacent current pattern. Other current patterns can also be implemented by slightly modifying the program in microcontroller and corresponding voltage data can be recorded.

The measured voltage data was transferred serially to computer system using serial communication, baud rate 9600, one start bit, 8 data bits and one stop bit. A program in VISUAL BASIC 2010 was written to maintain the serial communication between the data acquisition system and the computer system. The image reconstruction algorithms were implemented using EIDORS tool kit for MATLAB

The EIT system was tested and verified on a physical phantom and the results are presented in this chapter. The phantom was made from glass flask 16 cm diameter and 10 cm height. The system was design to use 16 electrodes made up of cupper and cylindrical in shape with 10cm height and 1mm diameter. The results were quite similar to those reported [88]. The reconstructed images clearly show the targets at the correct location although the shapes were not very clear. The resolution was best close to the edge and decreases as the target approaches the centre, as expected and observed before [87].

The developed system finds application in the field of biomedical instrumentation, non-destructive testing, flow measurement, geophysical prospecting cross borehole measurement *etc.* Algorithms used here can also be used for following purposes;

1. acoustic tomography
2. used along with acoustic as well as seismic measurements for determination of sub surface cavities
3. used as a prototype for EIT and laboratory for demonstration

CHAPTER SIX
Future Work

Further work is necessary on this project, some of which is described below.

6.1 Isolation

The power supply needs to be fully isolated from the mains supply as the existing power supply, is not approved for direct patient connection medical safety norms.

6.2 Adaptive Imaging Studies

All the images obtain from this hardware have been based on the adjacent current pattern which is not the best or optimal. Some improvements in the images is expected when optimal current patterns are used.

6.3 Multi-frequency Imaging Studies

Current system was based on the direct current approach which is not suitable for the medical purpose as it is has a problem of depolarization of the tissues in the human body. An alternating current of different frequencies should be used for getting much better image qualities. And for distinguishing different body tissues as the different tissues have different resistivity to different frequencies.

6.4 Clinical Experiments

For the system to be useful in a medical environment, it is necessary to carry out experiments to determine whether medical conditions can be accurately assessed. Currently it has been stated [89] that existing EIT methods have not been as effective as standard X-radiography in assessing pulmonary oedema. As this is a likely application for EIT, it is important that tests should be carried out to determine the effectiveness of absolute imaging in this and other applications

Bibliography

[1] R.A. Williams and M.S Beck, 'Process tomography: principal, techniques and applications, Butterworth-heinemann, oxford, 1995.

[2] O. Dorn, H. Berter-Aguirre, J.C. Berryman, and G.C. Papanicolaou, 'A nonlinear inversion method for 3D electromagnetic imaging using adjoint fields', Inverse Problem 15(1999), no.6, 1523-1558.

[3] M. Betrero and p. Boccacci, 'Introduction to inverse problems in imaging, IoP', Bristol, 1998.

[4] F. Natterer, 'The mathematics of computerization tomography', Wily, New York, 1986.

[5] Dickin F, Wang M, Electrical resistance tomography for process tomography, Meas Sci Tech, 1996, 7, 247-260.

[6] Alessandrini G, Rondi L, Stable determination of a crack in a planar inhomogeneous conductor, SIAM J Math Anal, 1998, 30, 326-340.

[7] Loke MH, Electrical imaging surveys for environmental and engineering studies-A practical guide to 2D and 3D surveys, 1997, Short training course lecture notes. Universiti Sains Malaysia, Penang, Malaysia.

[8] Polydorides N, Lionheart WRB, A MATLAB based toolkit for three-dimensional Electrical Impedance Tomography: A contribution to the EIDORS project, Measurement Science and Technology, 2002, 13, 1871-1883.

[9] Harris ND, Brown BH, Barber DC, Continuous monitoring of lung ventilation with electrical impedance tomography, Med Biol Soc, 1992, 1754-1755.

[10] Frerichs I, Hahn G, Hellige G, Thoracic Electrical Impedance Tomographic Measurements During Volume Controlled Ventilation-Effects of Tidal Volume and Positive End- Expiratory ressure, IEEE Trans. Medical Imag, 18, 768-778, 1999.

[11] Kunst PWA, Vonk Noordegraaf A, Hoekstra OS, Postmus PE, de Vries PMJM, entilation and perfusion imaging by electrical impedance tomography: A comparison with radionuclide scanning, Physiol Meas, 1998, 19, 481-490.

[12] Ey¨uboglu BM, Brown BH, Barber DC, In vivo imaging of cardiac related impedance changes, IEEE Eng Med Biol Mag, 1989, 8, 3945.

[13] Kerrouche N, McLeod CN, Lionheart WRB, Time series of EIT chest images using singular value decomposition and fourier transform. Physiol Meas, 2001, 22, 147-157.

[14] Holder DS, Electrical impedance tomography of brain function, Brain Topography, 1992, 5, 87-93.

[15] Gibson A, Bayford RH, Holder DS, Two-dimensional finite element modelling of neonatal head, Physiol Meas, 2000, 21, 45-52.

[16] Smallwood RH, Mangnall YF, Leathard AD, Transport of gastric contents, Physiol Meas, 1994, 15, 175-188.

[17] Barber DC, Brown BH and Freeston IL, Imaging spatial distributions of resistivity using applied potential tomography, Electronics Letters, 19, pp 933-5, 1983.

[18] Brown BH, Tissue impedance methods, Imaging with non-ionising radiation, Jackson DF (ed), Surrey Univ. Press, pp 85-110, 1983.

[19] British Standards Institution, Medical electrical equipment part 1, general requirements for safety, BS5724.

[20] Newell JC, Gisser DG and Isaacson D, An electric current tomograph, IEEE Trans. Biomed. Eng., BME-35, 10, pp 828-32, 1988.

[21] Zhu QS, Precision electrical impedance tomography instrumentation, PhD thesis, Oxford Brookes University, 1992.

[22] Brown BH, Barber DC, Leathard AD, Lu L, Wang W, Smallwood RH and Wilson AJ, High frequency EIT data collection and parametric imaging, Innov. Tech. Biol. Med., 15, No spécial 1, pp 1-8, 1994.

[23] Rui P, Lozano A and Pallas-Areny R, A broadband system for multifrequency static imaging in electrical impedance tomography, Clin. Phys. Physiol. Meas., 13, Suppl. A, pp 61-5, 1992.

[24] Leung HTL, Development of an electrical impedance tomograph for complex impedance imaging, PhD thesis, the Polytechnic of Wales, 1991.

[25] Jossinet J and Trillaud C, A high-contrast dual frequency multi-electrode system for electrical impedance tomography, Proceedings of a meeting on electrical impedance tomography, Copenhagen, pp 144-9, 1990.

[26] Shi Y, Rigaud B, Marsili PM, Morucci JP, An electrical impedance tomograph: hardware, software and static images, Proceedings of a meeting on electrical impedance tomography, Copenhagen, pp 150-7, 1990. 186

[27] Smith RWM, Design of a real-time imaging system for medical applications, PhD thesis, University of Sheffield, 1990.

[28] Zhang Z and Griffiths H, Dual-frequency electrical impedance tomography of the forearm, Proceedings of a meeting on electrical impedance tomography, Copenhagen, pp 257-62, 1990.

[29] Record PM, Single-plane multifrequency electrical impedance instrumentation, Physiol. Meas., 15, Suppl.A, pp 29-35, 1994.

[30] Gersing E and Osypka A, EIT using magnitude and phase in an extended frequency range, Physiol. Meas., 15, Suppl. A, pp 21-8, 1994.

[31] Cusick G, Holder DS, Birkett A and Boone K, A system for impedance imaging epilepsy in ambulator human subjects, Innov. Tech. Biol. Med., 15, No Spécial 1, pp 33-9, 1994.

[32] Brown BH, Barber DC and Seagar AD, Applied potential tomography: possible clinical applications, Clin. Phys, Physiol. Meas., 6, No.2, pp 109-21, 1985.

[33] Murphy D, Burton P, Coombs R, Tarassenko L and Rolfe P, Impedance Imaging in the Newborn, Clin. Phys. Physiol. Meas., 8, Suppl. A, pp 131-40, 1987.

[34] Griffiths H and Ahmed A, Applied Potential Tomography for Noninvasive Temperature Mapping in Hyperthermia, Clin. Phys. Physiol. Meas., 8, Suppl. A, pp 147-53, 1987.

[35] Sakamoto K and Kanai H, Electrical characteristics of flowing blood, IEEE Trans. Biomed. Eng., BME-20, 12, pp 686-95, 1979.

[36] Holder DS, Boone K and Cusick G, Specification for an electrical impedance tomogram for imaging epilepsy in ambulatory human subjects, Innov. Tech. Biol. Med., 15, No. spécial 1, pp 25-32, 1994. 187

[37] Mangnall YF, Baxter AJ, Avill R, Bird NC, Brown BH, Barber DC, Seagar AD, Johnson AG and Read NW, Applied potential tomography: a new non-invasive technique for measuring gastric function, Clin. Phys. Physiol. Meas., 8, Suppl. A, pp 119-129, 1987.

[38] Smith RWM, Brown BH, Freeston IL and McArle FJ, Real-time electrical impedance tomography, Proceedings of a meeting on electrical impedance tomography, Copenhagen, pp 212-6, 1990.

[39] Newell JC, Isaacson D, Cheney M, Saulnier GJ, Gisser DG, Goble JC, Cook RD, Edic PM and Newton CA, In vivo impedance images using sinusoidal current patterns, IEEE-EMBS, 14, 1992.

[40] Henderson RP and Webster JG, An impedance camera for spatially specific measurements of the thorax, IEEE Trans. Biomed. Eng, BME-25, 3, pp 250-4, 1978.

[41] Brown BH and Seagar AD, The Sheffield data collection system, Clin. Phys. Physiol. Meas., 8, Suppl. A, pp 91-7, 1987.

[42] Barber DC, Brown BH and Freeston IL, Experimental results of electrical impedance imaging, Proceedings of the Vth international conference on electrical bio-Impedance, Zadar, pp 1-5, 1983.

[43] Barber DC and Brown BH, Recent developments in applied potential tomograph - APT, Information processing in medical imaging, Proc. 9th Conf., Washington DC, pp 106-21, 1985.

[44] Harris ND, Suggett AJ, Barber DC and Brown BH, Applications of applied potential tomography (APT) in respiratory medicine, Clin Phys. Physiol. Meas., 8 Suppl. A, pp 155-65, 1987.

[45] Eyuboglu BM, Brown BH, Barber DC and Seagar AD, Localisation of cardiac related impedance changes in the thorax, Clin Phys. Physiol. Meas., 8, Suppl. A, pp 167-73, 1987. 188

[46] Conway J, Electrical impedance tomography for thermal monitoring of hyperthermia treatment: an assessment using in vitro and in vivo measurements, Clin. Phys, Physiol. Meas., 8, Suppl. A, pp 141-6, 1987.

[47] Kim Y, Webster JG and Tompkins WJ, Electrical impedance imaging of the thorax, Journal of Microwave Power, 18(3), pp 245-57, 1983.

[48] Yorkey TJ and Webster JG, A comparison of impedance tomographic reconstruction algorithms, Clin. Phys. Physiol. Meas., 8, Suppl. A, pp 55-62, 1987.

[49] Tarrasenko L and Rolfe P, Imaging spacial distributions of resistivity – an alternative approach, Electronics Letters, 20, pp574-5, 1984.

[50] Griffiths H and Ahmed A, A dual-frequency applied potential tomography technique:computer simulations, Clin. Phys. Physiol. Meas., 8, Suppl. A, pp 103-7, 1987.

[51] Griffiths H, Leung HTL and Williams RJ, Imaging permittivity in electrical impedance tomography, IEEE-EMBS, 13, pp 16-7, 1991.

[52] Riu P, Rosell J and Pallas Areny J, In vivo static imaging for the real and the reactive parts in electrical impedance tomography using multifrequency techniques, IEEE-EMBS, 14, pp 1706-7, 1992.

[53] Liu P, Griffiths H, Wiles C M, Nathadwarawala KM and Stewart W, Measurement of pharyngeal transit time by electrical impedance tomography, Clin. Phys. Physiol. Meas., 13, Suppl. A, pp 197-200, 1992.

[54] Holder DS, Feasibility of developing a method of imaging neuronal activity in the human brain: a theoretical review, Med. & Biol. Eng. & Comput., 25, pp 2-11, 1987.

[55] Rao A, Hanquan Y and Holder DS, Imaging sensory and visual evoked responses in the brain with electrical impedance tomography and cortical electrodes, Proceedings of the 9th ICEBI, Heidelberg, pp 472-3, 1995. 189

[56] Brown BH, Sinton AM, Barber DC, Leathard AD and McArdle FJ, Simultaneous display of lung ventilation and perfusion on a real-time EIT system, IEEE-EMBS, 14, pp 1710-11, 1992.

[57] Gisser DG, Isaacson D, and Newell JC, Current topics in impedance imaging, Clin. Phys. Physiol. Meas., 8, Suppl. A, pp 39-46, 1987.

[58] Breckon WR and Pidcock MK, Mathematical aspects of impedance imaging, Clin. Phys. Physiol. Meas., 8, Suppl. A, pp 77-84, 1987.

[59] Gisser DG, Isaacson D and Newell JC, Theory and performance of an adaptive current tomography system, Clin. Phys. Physiol. Meas., 9, Suppl. A, pp 35-41, 1988.

[60] Cheney M, Isaacson D, Newell JC, Simske S, and Goble J, NOSER: An algorithm for solving the inverse conductivity problem, International Journal of Imaging Systems and Technology, 2, pp 66-75, 1990.

[61] Saulnier GJ, Cook RD, Gisser DG, Goble JC, Hochgraf CG, Isaacson D and Newell JC, A high-speed high-precision electrical impedance tomograph, IEEE-EMBS, 13, pp 5-6, 1991.

[62] Avis NJ and Barber DC, Adjacent or polar drive? : Image reconstruction implications in electrical impedance tomography systems employing filtered back projection, IEEE-EMBS, 14, pp 1689-90, 1992.

[63] Avis NJ and Barber DC, Image reconstruction using non-adjacent drive configurations, Physiol. Meas., 15, Suppl. A, pp 153-60, 1994.

[64] Dines KA, and Lytle RJ, Analysis of electrical conductivity imaging, Geophysics, 46, pp 1025-36, 1981.

[65] Yorkey et al, Comparing reconstruction algorithms for electricalimpedance tomography, IEEE Trans. Biomed. Eng., BME-34, 11, pp 843-52, 1987.

[66] Cheney M et al, NOSER: An algorithm for solving the inverse conductivity problem, International Journal of Imaging Sytems and Technology, 2, pp 66-75, 1990.

[67] Paulson K, Breckon W and Pidcock M, Optimal measurements in electrical impedance tomography, IEEE-EMBS, 14, pp 1730-1, 1992.

[68] Cheney M and Isaacson D, A layer-stripping algorithm for impedance imaging, IEEE-EMBS, 13, pp 3-4, 1991.

[69] Breckon WR and Pidcock, MK, Data errors and reconstruction algorithms in electrical impedance tomography, Clin. Phys. Physiol. Meas., 9, Suppl. A, pp 105-9, 1988.

[70] Paulson KS, Breckon WR and Pidcock MK, A hybrid phantom for electrical impedance tomography, Clin. Phys. Physiol. Meas., 13, Suppl. A, 155- 61, 1992.

[71] McLeod CN, Shi Y, Denyer CW, Lidgey FJ, Lionheart WRB, Paulson KS and Pidcock MK, Chest impedance imaging using trig. current patterns, Proceedings of the 9th ICEBI, Heidelberg, pp 408-9, 1995.

[72] Vauhkonen M, LionheartWR B, Heikkinen L M, auhkonen P J and Kaipio J P,"A MATLAB package for the EIDORS project to reconstruct two-dimensional EIT images" Physiol. Meas. 22 107-111, 2000.

[73] Vauhkonen M, " Electrical impedance tomography and prior information", PhD thesis, University of Kuopio, Finland, 1997.

[74] Polydorides N and Lionheart W R B, “A Matlab toolkit for three-dimensional electrical impedance tomography: a contribution to the Electrical Impedance and Diffuse Optical Reconstruction Software project”, Meas. Sci. Technol. 13 1871-1883, 2002.

[75] Polydorides N, “Image reconstruction algorithms for soft-field tomography”, Ph.D. Thesis, University of Manchester Institute of Science and Technology, U.K, 2002.

[76] Adler A and Guardo R, “Electrical impedance tomography: regularised imaging and contrast detection”, IEEE Trans. Med. Imaging 15 170-9, 1996.

[77] Borsic A, “Regularisation Methods for Imaging from Electrical Measurements” PhD thesis, Oxford Brookes University, U.K, 2002.

[78] Soleimani M Gomez-Laberge C and Adler A, “Imaging of conductivity changes and electrode movement in EIT”, Physiol. Meas., submitted, 2005.

[79] Asfaw Y and Adler A, “Automatic detection of detached and erroneous electrodes in electrical impedance tomography”, Physiol. Meas., 26 S175-S183, 2005.

[80] Free Software Foundation, GNU General Public Licence Boston MA USA http://www.gnu.org/copyleft/gpl.html, 1991.

[81] Cederqvist P, “Version Management with CVS”, Network Theory Ltd, Bristol, UK, 2002.

[82] Eaton J W, “Gnu Octave Manual”, Network Theory Ltd, Bristol, UK, 2002.

[83] Gamma E Helm R Johnson R and Vlissides J, “Design Patterns: Elements of Reusable Object- Oriented Software Addison-Wesley”, Boston, MA, USA, 1995.

[84] Ramachandran P, “Scientific data visualization with MayaVi Conf. SciPy: Python for Scientific Computing Pasadena”, CA, USA http://mayavi.sf.net/, 2003.

[85] Schoberl J, “NETGEN - An advancing front 2D/3D-mesh generator based on abstract rules”. Comput. Visual. Sci 1 41-52 http://www.hpfem.jku.at/netgen/, 1997.

[86] A. Adler, W.R. B. Lionheart , ‘Uses and abuses of EIDORS: An extensible software base for EIT’.

[87] Cook RD, Saulnier GJ, Gisser DG, Goble JC, Newell JC and Isaacson D, ACT3: a high-speed, high precision electrical impedance tomograph, IEEE Trans. Biomed. Eng., BME-41, 8, pp 713-22, 1994.

[88] C.W.L DENYER, “Electronics For Real-Time And Three Dimensional Electrical Impedance”, PhD thesis, Oxford Brookes University, 1996

[89] Holder DS, Biomedical applications of EIT: a shopping list for clinicians and engineers, presentation at the 5th European Community workshop on electrical impedance tomography, Barcelona 1993.